ARMY RESEARCH LABORATORY

Parabolized Navier-Stokes Computation of Surface Heat Transfer Characteristics for Supersonic and Hypersonic KE Projectiles

Bernard J. Guidos
Paul Weinacht

ARL-TR-191 August 1993

NOTICES

Destroy this report when it is no longer needed. DO NOT return it to the originator.

Additional copies of this report may be obtained from the National Technical Information Service, U.S. Department of Commerce, 5285 Port Royal Road, Springfield, VA 22161.

The findings of this report are not to be construed as an official Department of the Army position, unless so designated by other authorized documents.

The use of trade names or manufacturers' names in this report does not constitute indorsement of any commercial product.

REPORT DOCUMENTATION PAGE

Form Approved
OMB No. 0704-0188

1. AGENCY USE ONLY (Leave blank)	2. REPORT DATE	3. REPORT TYPE AND DATES COVERED
	August 1993	Final, September 1991 - April 1993

4. TITLE AND SUBTITLE

PARABOLIZED NAVIER-STOKES COMPUTATION OF SURFACE HEAT TRANSFER CHARACTERISTICS FOR SUPERSONIC AND HYPERSONIC KE PROJECTILES

5. FUNDING NUMBERS

PR: 1L162618AH80
WO: 62618A-00-001 AJ

6. AUTHOR(S)

BERNARD J. GUIDOS and PAUL WEINACHT

7. PERFORMING ORGANIZATION NAME(S) AND ADDRESS(ES)

US Army Research Laboratory
ATTN: AMSRL-WT-PB
Aberdeen Proving Ground, MD 21005-5066

8. PERFORMING ORGANIZATION REPORT NUMBER

9. SPONSORING/MONITORING AGENCY NAME(S) AND ADDRESS(ES)

US Army Research Laboratory
ATTN: AMSRL-OP-CI-B (Tech Lib)
Aberdeen Proving Ground, Maryland 21005-5066

10. SPONSORING/MONITORING AGENCY REPORT NUMBER

ARL-TR-191

11. SUPPLEMENTARY NOTES

This report supersedes BRL-IMR-970, April 1992.

12a. DISTRIBUTION/AVAILABILITY STATEMENT

Approved for public release; distribution is unlimited.

12b. DISTRIBUTION CODE

13. ABSTRACT (Maximum 200 words)

Perfect gas heat transfer characteristics are presented for two existing supersonic finned kinetic energy (KE) projectiles (M735 and M829) and for a conceptual hypersonic KE projectile configuration. The hypersonic configuration is obtained by replacing the fins of the M829 with a conical flare of varying sweep angle. A three-dimensional, viscous, parabolized Navier-Stokes (PNS) computational technique is used to compute the perfect gas adiabatic wall temperatures and heat transfer rates in the velocity range 1.3 km/sec to 4 km/sec (Mach number range about 4 to 12). The heat transfer characteristics provide a necessary boundary condition for subsequent heat conduction computations, which simulate the transient in-flight thermal response of projectile configurations.

14. SUBJECT TERMS

Computational fluid dynamics; convection heat transfer; aerodynamic heating; supersonic flow; turbulent flow.

15. NUMBER OF PAGES

49

16. PRICE CODE

17. SECURITY CLASSIFICATION OF REPORT	18. SECURITY CLASSIFICATION OF THIS PAGE	19. SECURITY CLASSIFICATION OF ABSTRACT	20. LIMITATION OF ABSTRACT
UNCLASSIFIED	UNCLASSIFIED	UNCLASSIFIED	UL

INTENTIONALLY LEFT BLANK.

ACKNOWLEDGMENTS

The authors thank Dr. Walter B. Sturek and Mr. Harris L. Edge for reviewing the report, and Miss Jennifer J. Schnell for providing assistance with the computer data and graphics.

INTENTIONALLY LEFT BLANK.

TABLE OF CONTENTS

INTENTIONALLY LEFT BLANK.

LIST OF FIGURES

INTENTIONALLY LEFT BLANK.

LIST OF TABLES

INTENTIONALLY LEFT BLANK.

1. INTRODUCTION

The U.S. Army is currently devoting a large amount of resources to the development of future generations of launch systems. The projectiles to be launched will travel at hypersonic velocities, well above Mach 5. One major problem at these velocities is that the fins on existing kinetic energy (KE) projectiles can be expected to fail because of excessive heating and structural loading. The new families of hypervelocity KE projectiles must possess satisfactory aerodynamic characteristics to achieve increased terminal performance, yet withstand the hostile launch and flight environments of the hypersonic flow regime.

The aerodynamic research for the hypervelocity program is focusing on several critical aspects of projectile performance, including (1) drag and its various components, (2) pitch-plane static and dynamic stability, (3) surface heat transfer, (4) thermal response, and (5) real gas effects. The U.S. Army Research Laboratory (ARL) continues to develop and apply complex three-dimensional computational fluid dynamics (CFD) models to predict each of these aerodynamic phenomena. The latest challenge is to apply and extend these capabilities to higher velocities than previously attempted in-house and impact the design of the new class of hypervelocity projectiles.

The primary objective of this report is to present recent CFD results of surface heat transfer characteristics for two existing supersonic finned KE projectiles (M735 and M829) and for a conceptual hypersonic flared KE projectile configuration. The in-flight surface heat transfer is a necessary boundary condition in the simulation of projectile thermal response. Results for the M735 and M829 projectiles are presented for their respective service velocities (both less than Mach 5). Results for the hypersonic configuration are presented for velocities approaching Mach 12 (about 4 km/sec). By comparing results for these three configurations, an appreciation is gained for differences in heating characteristics attributable to higher launch velocities, as well as differences between fins and flares. The computational approach is a parabolized Navier-Stokes (PNS) technique, and the methodology and relevant issues of this technique for computing surface heat transfer characteristics are addressed herein.

2. A NOTE ABOUT BLUNT NOSETIP HEATING

The determination of in-flight surface heat transfer characteristics on the blunt nosetip has long been an important element in projectile design. A literature search will verify that, 30 years ago, much effort was expended on the problem of nosetip heating and ablation for re-entry vehicles. Currently, many U.S. Army KE projectiles possess steel nosetips that

prevent ablation from occurring. Research into new materials is being pursued to protect the projectile nosetips from ablation at the higher launch velocities expected to be reached.

In this regard, it is emphasized here that in-house work is ongoing to maintain a capability to model blunt nosetip aerodynamic heating at hypersonic speeds, including real gas effects. However, the work to be reported here assumes a pointed conical nosetip, and attention focuses on the KE projectile forebodies (i.e., the cone and cylinder) as well as the fins and flares. Future modeling efforts will examine the downstream effects of blunt nosetip heating, using the coupling approach reported in a previous research effort (Guidos, Weinacht, and Dolling 1990).

3. HEAT TRANSFER ANALYSIS

The main objective in this report is to compute the perfect gas surface heat transfer characteristics for KE projectile configurations at supersonic and hypersonic speeds. The current approach is to compute the surface distributions of adiabatic wall temperature and heat transfer over the entire projectile surface. The CFD technique is described in a later section. The heat transfer analysis begins with a quick review of relevant quantities to be used, for which clear definitions and conventions are essential.

3.1 Adiabatic Wall Temperature. The adiabatic wall temperature, T_{aw}, can be defined as the surface temperature (or temperature distribution) for which no heat transfer occurs between the body and the fluid. The classical treatment of perfect gas adiabatic wall temperature (Schlichting 1962) addresses the simpler case of flow over a flat plate. The adiabatic wall temperature is characterized in terms of the boundary-layer edge conditions (which, in boundary layer theory, are synonymous with free-stream conditions). This well-known relationship is written here as

$$T_{aw} = T_e(1 + r\frac{\gamma - 1}{2}M_e^2) \tag{1}$$

in which M_e is the edge Mach number, T_e is the edge temperature, and r is the recovery factor. An equivalent expression is obtained from Eq. (1) by employing the stagnation relationships of compressible flow theory (Zucrow and Hoffman 1976), yielding

$$T_{aw} = T_e + r(T_o - T_e) \tag{2}$$

in which T_o is the edge total temperature.

For incompressible, laminar air flow over flat plates, boundary layer theory shows the recovery factor to be equal to the square root of the Prandtl number (i.e., $r = (P_r)^{1/2} \approx$

$(0.72)^{1/2} \approx 0.85$). In support of this finding, Truitt (1960) cites laminar boundary layer studies over a flat plate (Emmons and Brainard 1942) where the recovery factor was found to vary almost exactly as the square root of the Prandtl number. Also, Schlichting shows experimentally derived values (Eber 1952) of recovery factor for compressible, laminar air flow over cones for Mach numbers 1.5 to 4.6 and cone half-angles 5° to 40°, and the theoretical prediction of $r = \sqrt{P_r}$ is seen to be confirmed well within 5%.

In the case of turbulent air flow, Truitt cites flow measurements (Ackermann 1942) which conclude that the recovery factor is approximately equal to the cube root of the Prandtl number (i.e., $r \approx (P_r)^{1/3} \approx (0.72)^{1/3} \approx 0.9$). For turbulent flow over a cone at Mach 3.1, Schlichting presents data (Evvard, Tucker, and Burgess 1954) which show $r = 0.88$ downstream of boundary layer transition. In all, a large number of sources can be found in the literature supporting the aforementioned relationships between r and P_r.

This information is significant because it says, to a large extent, that the perfect gas adiabatic wall temperature can be calculated with confidence if the edge conditions of the boundary layer of interest are known. For simple flows, this concept is helpful since the required edge conditions can be calculated using simplified theories. However, the edge conditions of flows over complex configurations such as KE projectiles are not easily (or accurately) calculated using simple theories, and so the usefulness of the recovery factor becomes less certain. A relevant pursuit is to examine the utility of the common engineering assumption of an adiabatic wall temperature based on free-stream conditions rather than edge conditions, that is,

$$T_{aw} = T_\infty(1 + r_f \frac{\gamma - 1}{2} M_\infty^2) \tag{3}$$

in which r_f is the recovery factor applied to free-stream conditions.

3.2 Surface Heat Transfer Coefficient. The local vector of surface heat transfer rate per unit area, $\bar{q}$, is obtained from the computed flowfield solutions using Fourier's Law, that is,

$$\bar{q} = -k(\frac{\partial T}{\partial n}) \mid_{wall} \bar{e}_n \tag{4}$$

in which k is the coefficient of thermal conductivity of the fluid, $\bar{e}_n$ is the unit vector perpendicular to the body surface, and n is the physical coordinate along $\bar{e}_n$. The rate of heat transfer from the fluid to the body per unit area, q, is defined as

$$q = -\bar{q} \cdot \bar{e}_n \tag{5}$$

The local heat transfer rate is obtained from the computed flow fields by applying Eq. (4) as a second order, one-sided, finite difference approximation along the transformed coordinate

extending outward from the wall (i.e., the ζ coordinate, which is formally introduced in the next section).

The local surface heat transfer coefficient is defined by applying Newton's Law of Cooling, written here as

$$h = \frac{q}{T_{aw} - T_w} \tag{6}$$

in which q is the local heat transfer rate that occurs for a specified wall temperature T_w. Once h is adequately defined using Eq. (6), it can be used, along with T_{aw}, as a boundary condition in separate heat conduction computations. Heat conduction computations normally require a model of heat transfer on the projectile surface, because computational power does not yet exist which would allow a feasible coupling of the aerodynamic computations and the heat conduction computations. If these two CFD analyses could be fully coupled, then the instantaneous surface heat transfer and internal heat conduction could be calculated directly and with the most accuracy. Such a coupled aerothermodynamics approach is desirable as a long-term goal for this problem.

In summary, then, the current approach is to use CFD to compute surface distributions of q and T_{aw} at Mach numbers that bracket the flight trajectory to be simulated. These values of q and T_{aw} are then combined to form surface distributions of h at each Mach number. The quantities h and T_{aw} can then be employed in separate in-flight heat conduction computations to simulate the transient thermal response of the projectile.

4. CFD BACKGROUND

The three-dimensional, viscous flow results presented here were computed using a parabolized Navier-Stokes (PNS) computational technique on a Cray X-MP/48 supercomputer located at Aberdeen Proving Ground. The PNS technique, which has been extensively used and developed in-house, is a powerful CFD research tool for supersonic and hypersonic projectile configurations. The PNS technique is a space marching (as opposed to a time marching) technique; that is, one numerical integration sweep is made from the nosetip of the projectile to the base to obtain a single steady state solution. As a result, a solution for a three-dimensional geometry at angle of attack may be generated using about an hour or two of CPU time on a Cray X-MP. Axisymmetric configurations at 0° angle-of-attack flight conditions may take less than 10 minutes. Time-marching techniques, on the other hand, may take days or weeks of computer time on a Cray X-MP or Cray-2 to obtain a solution over an entire projectile surface, excluding the base.

The PNS technology was first applied in-house (at the former U.S. Army Ballistic Re-

search Laboratory [BRL]) to compute static pitch-plane and Magnus coefficients for spinning and non-spinning shell and for wind tunnel models at various angles of attack (Sturek and Schiff 1981; Schiff and Sturek 1981). Similar applications were made to shell at moderate angle of attack and to finned KE projectiles (Weinacht et al. 1985, 1986). The technique was modified to compute roll characteristics of finned KE projectiles with exact fin geometry using a rotating coordinate frame (Weinacht and Sturek 1988). The technique was further advanced to compute the pitch damping of finned projectiles (Weinacht and Sturek 1990) and axisymmetric configurations (Weinacht, Sturek, and Schiff 1991) using coning motion. A number of other BRL publications that report applications of the PNS technique to projectile aerodynamics have also been published during this time frame but are not formally mentioned here.

Almost all previous in-house work with PNS was directed toward the prediction of aerodynamic force and moments, rather than heat transfer. But recently, with renewed interest in achieving higher launch velocities into the hypersonic regime, the PNS technique has once again surfaced as a valuable commodity for obtaining three-dimensional, viscous flow results. The main obstacles for this task pertain to the careful application of the technique; that is, resolving the boundary layer, generating converged cone start solutions, obtaining oscillation-free solutions with minimal artificial smoothing, and eventually assessing real gas effects.

Previous in-house CFD work involving surface heat transfer of projectiles is worth mentioning for purposes of perspective. Computational assessment of heat transfer on nosetips and fins was first performed in-house using a computer program known as the ABRES Shape Change Code - or ASCC (Sturek, et al. 1983; Sturek, Kayser, and Weinacht 1983). The ASCC code was originally developed by Acurex Corporation as a fast, inexpensive way to predict heat transfer, thermal response, and ablation of axisymmetric geometries (i.e., nosetips) and 2-D planar geometries (i.e., fins). Some recent developments and details of the ASCC code can be traced in BRL contract reports by Suchsland (1981), Kobayashi (1984), and Strawn and Kobayashi (1984).

A more rigorous CFD approach for modeling fin thermal response was applied by Weinacht, Sturek, and Wooden (1984). This approach solved the two-dimensional, unsteady heat conduction equation with a second order accurate, partially implicit finite difference technique which was initially developed in part by Dwyer, Kee, and Sanders (1980). For that study, the in-flight surface heat transfer boundary condition was supplied by the ASCC code.

A set of PNS computations worth mentioning here was sponsored by the U.S. Army and published by Thermal Sciences, Inc. (Nicolet and Srinivasan 1982). That study attempted

to assess real gas effects for a cone-cylinder configuration at Mach 10. The authors cautioned that the grid resolution at the body surface might not have been adequate and expressed uncertainty about the effect of artificial smoothing parameters. The authors concluded that real gas effects may be important near the nosetip but not farther downstream. It should be noted that perfect gas blunt nosetip solutions from the code reported by Kutler, Pedelty, and Pulliam (1980) were used as starting solutions for both the perfect gas and real gas PNS solutions.

The PNS code was used to compute heat transfer for an M735 configuration by Balakrishnan and Weinacht (1986). The differences between perfect gas and real gas models were examined by implementing engineering correlations for transport properties into the PNS code. The real gas results showed an increase in heat transfer rate (as much as a 12%, even at Mach 3) compared to the perfect gas results.

More recently, the effort to model in-flight thermal response of KE projectile fins using three-dimensional and quasi-three-dimensional heat conduction codes (Sturek, Sturek, and Ferry 1990; Sturek, Dwyer, and Ferry 1990) once again raised the need for accurate heat transfer rates. ASCC code results were used in one study; PNS results were used in the other. The PNS results, referenced in the report by Sturek, Sturek, and Ferry (1990) as private communication, were performed for the M829 projectile in-house by Weinacht but were never formally published. The PNS results to be presented in this report were generated independently from those used by Sturek, Sturek, and Ferry (1990).

Finally, the work of Nusca (1990) is acknowledged as an ongoing engineering approach for determining the aerothermodynamics of axisymmetric projectiles. That procedure uses the viscous-inviscid coupling approach, with an assortment of more classical inviscid methods available to the user.

5. COMPUTATIONAL APPROACH

5.1 PNS Numerical Technique. The PNS technique introduced by Schiff and Steger (1979) is a three-dimensional, finite difference, viscous flow solution procedure for attached supersonic/hypersonic flow fields. The PNS technique spatially integrates the dimensionless, transformed, steady, thin-layer, mass-averaged Navier-Stokes equations in strong conservation law form. The Cartesian form of the governing equations represents steady-state conservation of mass, momentum, and energy in transformed coordinates for large Reynolds number flows and is written as

$$\frac{\partial \hat{E}_s}{\partial \xi} + \frac{\partial \hat{F}}{\partial \eta} + \frac{\partial \hat{G}}{\partial \zeta} = \hat{R}e^{-1}\frac{\partial \hat{S}}{\partial \zeta} \tag{7}$$

These equations were recast in cylindrical coordinates and applied by Rai and Chaussee (1983). The major advantage is that the cylindrical coordinate formulation requires only three circumferential grid planes for axisymmetric flow cases, within the framework of the bilateral symmetry which is imposed. The cylindrical form of the governing equations was used extensively in this study and is written as

$$\frac{\partial \hat{E}_s}{\partial \xi} + \frac{\partial \hat{F}}{\partial \eta} + \frac{\partial \hat{G}}{\partial \zeta} + \hat{H}_c = \hat{R}e^{-1}(\frac{\partial \hat{S}}{\partial \zeta} + \hat{S}_c) \tag{8}$$

The vectors $\hat{E}_s$, $\hat{F}$, and $\hat{G}$ contain the transformed inviscid fluxes. $\hat{E}_s$ is a modified flux vector resulting from the subsonic sublayer approximation (Schiff and Steger 1979). The vector $\hat{S}$ is the transformed vector of viscous terms that results from the thin-layer approximation. The vectors $\hat{H}_c$ and $\hat{S}_c$ contain inviscid and viscous source terms, respectively, resulting from the cylindrical coordinate formulation. The components of the vectors for the Cartesian formulation are given in many sources, including Schiff and Steger (1979). The components of all the vectors for the cylindrical formulation can be found in a report by Weinacht and Sturek (1990).

The transformed coordinates are

$\xi = \xi(x)$, the axial-like (marching) coordinate;

$\eta = \eta(x, y, z)$, the circumferential-like coordinate; and

$\zeta = \zeta(x, y, z)$, the outward coordinate.

The vector of dependent variables is

$$\bar{Q} = [\rho, \rho u, \rho v, \rho w, e] \tag{9}$$

in which the density is ρ; the axial, circumferential, and radial velocity components are are u, v, and w, respectively; and the total energy per unit volume is e. The solution is obtained at each grid point using the approximately-factored, implicit, delta-form, finite difference algorithm of Beam and Warming (1978). Second order central-differencing is used in the circumferential and radial directions, and first order one-sided differencing is used in the marching direction. The solution is advanced downstream by numerically integrating in the main flow direction. Each marching step requires a series of block tridiagonal matrix inversions (sweeps) in the circumferential and radial directions.

Initial conditions for marching are generated using the PNS method in step-back mode (Sturek and Schiff 1981), which assumes conical flow conditions near the nosetip and iteratively refines the solution to satisfy this assumption. Fourth order explicit smoothing terms are added to suppress high frequency oscillations. Second order implicit smoothing terms are added to maintain numerical stability in regions of large pressure gradients (such as fin leading edges).

Perfect gas behavior is assumed for all results presented in this report. Turbulence is accounted for using the two-layer, algebraic eddy viscosity model of Baldwin and Lomax (1978). In that model, the inner wall layer eddy viscosity is computed using a conventional Prandtl mixing length with Van Driest (1951) damping. The outer, or wake, layer eddy viscosity is based upon an evaluation of the maximum moment of vorticity and its distance from the wall.

The outer boundary, which consists of the bow shock, is shock fitted using the implicit procedure reported by Rai and Chaussee (1983). Bilateral symmetry conditions are imposed at the pitch plane.

5.2 Body Surface Boundary Conditions. The body surface boundary conditions are perhaps the most vital aspect of this application of the PNS technique. Extremely fine grid resolution is required at the body surface to accurately define the temperature gradients. An established adaptive grid technique (Sturek and Schiff 1980) is applied over the configuration to ensure this. The adaptive grid technique controls the distance from the wall of the interior grid points adjacent to the body. This is accomplished by monitoring the boundary-layer coordinate, y^+, defined as

$$y^+ = \frac{u_\tau n}{\nu_w} \tag{10}$$

in which u_τ is the shear velocity,

$$u_\tau = \sqrt{\tau_w / \rho_w}, \tag{11}$$

in which ν_w is the kinematic viscosity at the body surface, and τ_w is the shear stress at the body surface. The boundary-layer coordinate at the grid points adjacent to the body surface, y_1^+, is adjusted to stay within a specified range.

In direct conflict with this adaptive grid procedure are numerical limitations of the PNS code which restrict the minimum allowable resolution at the wall. The restrictions become pertinent in areas of severe pressure gradients, such as the fin leading edge, where numerical oscillations can occur if y_1^+ is too small. For this reason, it is important to implement temperature boundary conditions that perform consistently within the limits of grid resolution and numerical smoothing.

The body surface boundary conditions are applied both explicitly and implicitly. The explicit boundary conditions are applied directly to the dependent variables. The implicit boundary conditions are applied to the Jacobian matrices that relate the changes in dependent variables in the marching (ξ) direction. The implicit boundary conditions were applied with first order and second order accuracy, and no differences were found in the computed results. However, the explicit boundary conditions were found to have a noticeable effect on the computed results even for the finest grid resolutions used.

The explicit body surface boundary conditions are applied as follows. The no-slip condition is enforced ($u_w = v_w = w_w = 0$ throughout this study) and the pressure is held constant across the subsonic portion of the boundary layer (i.e., the subsonic sublayer approximation). The energy is defined from the pressure using the perfect gas law. The density boundary condition is applied differently for the two conditions of adiabatic wall and specified wall temperature, in the following manner:

(1) Adiabatic Wall Condition. To compute the adiabatic wall temperature, a zero heat transfer wall boundary condition is imposed, that is,

$$(\frac{\partial T}{\partial n}) \mid_{wall} = 0 \tag{12}$$

In the current PNS formulation, the n coordinate is assumed to be coincident with the ζ coordinate at the wall. It is noted that the current fin grid approach (Rai, Chaussee, and Rizk 1983; Weinacht, et al. 1985) satisfies this assumption everywhere except on the fin leading edge. In practice, the boundary condition is formulated as a zero density gradient in the ζ direction, and is applied using a one-sided difference. Therefore, in regions where large temperature gradients exist tangent to the body surface (i.e., at the fin leading edges), a small error is expected. It was confirmed that a second order explicit implementation of the density boundary condition was necessary to compute grid independent results for adiabatic wall temperature, even with y_1^+ as small as 1.0.

(2) Surface Temperature Condition. To compute the heat transfer rate, a constant surface temperature boundary condition is prescribed. The density is then determined from the temperature and pressure. The overriding consideration is to use the finest grid resolution possible at the wall without inflicting numerical instabilities into the solution. This approach, used with a second order, one-sided, finite difference evaluation of the temperature gradient, was found to be sufficient to achieve grid independent results for heat transfer. The heat transfer results to be presented here were all generated using the aforementioned adaptive grid technique, with a value of y_1^+ typically maintained at less than 0.5. The exception is at the fin leading edges, where y_1^+ was sometimes as high as 2.0 or 3.0.

6. CONFIGURATIONS AND FLIGHT CONDITIONS

Three different KE projectile configurations are examined here. The first two are fielded, fin-stabilized KE projectiles: the M735 and M829 KE rounds. The third is an M829-like cone-cylinder-flare configuration (identified here as F829) which is a conceptual hypervelocity projectile design.

The computational models of the M735 and M829 projectiles, Figures 1 and 2, are simplified versions of the actual models. Both models possess a conical nose section, followed by a cylindrical section of constant diameter. The reference diameters of the cylindrical sections are 35.2 mm and 27.05 mm, respectively. The total model lengths are about 14 calibers and 23 calibers (1 caliber = 1 cal = 1 reference diameter). Both models have six fins equally distributed around the body, aligned with the projectile axis, with fin angles 19° and 20.25°, respectively. The fins have cylindrically blunted leading edges, and the fin thicknesses are shown in the figures.

Other geometric simplifications are worth noting as follows. The sabot grooves on the cylindrical portion of the actual configurations are replaced with a smooth surface. No leading edge or trailing edge cuts are included. The juncture of the cylinder and the fin leading edge is modified with a small rounded fillet, which typically extends about 0.3 to 0.5 cal upstream and downstream of the juncture. The overhanging fin of the M829 is modeled with the cylinder extending to the fin trailing edge; the resulting fin gap is modeled as a solid structure.

The F829 configuration, Figure 3, is similar to the M829 configuration. The F829 is derived by replacing the fins of the M829 with a conical flare. Flare angles examined in this study vary from 0° to 20° in increments of 4°.

The flight conditions used for each of the configurations are shown in Tables 1 through 3. The higher velocities of the M735 and M829 configurations represent the service launch velocities for the 105mm and 120mm guns, as given in Department of the Army Firing Tables FT 105-A-3, C-1 and FT 120-D-1, respectively. The lower velocities represent the respective flight velocities at a range of 3000 meters. In all cases, atmospheric, sea level, free-stream conditions are assumed. The angle of attack is fixed at 0°, and the spin rate is fixed at 0 rpm.

For the heat transfer computations, the wall temperature is specified as 294 K unless otherwise indicated. It is noted that recent in-house heat conduction simulations (Sturek, Sturek and Ferry 1990; Sturek, Dwyer, and Ferry 1990) indicate that the spatial variation of wall temperature over the fin surface is quite pronounced, even at gun tube exit. Toward this

Table 1. Flight Conditions for M735 Configuration

Mach No.	Velocity (m/sec)	Reynolds No. (Re_m)	Time of Flight (sec)	Range (m)
4.36	1500	9.88×10^7	0.0	0.0
3.78	1300	8.58×10^7	2.1	3000.0

Table 2. Flight Conditions for M829 Configuration

Mach No.	Velocity (m/sec)	Reynolds No. (Re_m)	Time of Flight (sec)	Range (m)
4.9	1670	11.1×10^7	0.0	0.0
4.36	1490	9.88×10^7	1.9	3000.0

end, some additional results are presented for the M735 with wall temperatures higher than the atmospheric value. The effect of spatially varying surface temperature on heat transfer rate is not specifically addressed but may be a topic for future study.

Fully turbulent flow conditions are assumed for all computations. Though the effect of boundary-layer transition from laminar to turbulent flow is of definite interest, the prediction of transition for general flow problems is beyond the present state-of-the-art in CFD. The state of the boundary-layer on the fins of the configurations of this study is not known for certain. However, the heat transfer rate for the fully turbulent flow condition serves as an upper bound for the aerodynamic heating expected to occur in actual flight. The determination of the laminar and transitional heat transfer rates is an area of future research.

7. RESULTS

7.1 M735 Projectile - Adiabatic Wall Temperature. The first results to be presented are the computed adiabatic wall temperatures for the M735 projectile. Figures 4 and 5 show the computed perfect gas adiabatic wall temperature over the M735 projectile forebody and fin leading edge at Mach numbers 4.36 and 3.78, respectively. Discounting the spikes that occur in the computed distribution, the computed adiabatic wall temperature in each case varies by about 4% over the forebody and fin leading edges. The spikes are believed to be numerical effects arising from the sensitivity of the adiabatic wall boundary condition. The boundary condition is considered sensitive because it is based partly on a numerically valued derivative (in this case, $\partial T/\partial n$).

Table 3. Flight Conditions for F829 Configuration

Mach No.	Velocity (m/sec)	Reynolds No. (Re_m)
11.8	4000	26.8×10^7
8.8	3000	20.0×10^7
5.9	2000	13.4×10^7
4.4	1500	9.96×10^7

Also shown in Figures 4 and 5 are reference adiabatic wall temperatures that have been calculated using different free-stream temperature recovery factors (see Eq. (3)). These temperatures are marked with their corresponding free-stream recovery factor. The inclusion of these values demonstrates that free-stream conditions, along with recovery factors in the range of 0.86 to 0.89, can provide a useful engineering approximation of perfect gas adiabatic wall temperature consistent with both the PNS results and the classical boundary-layer treatment.

Figures 6 and 7 show the computed chordwise distributions of adiabatic wall temperatures. The temperatures are plotted as a function of axial distance from the leading edge. At these spanwise locations, the computed distributions vary by only a few percent from leading edge to trailing edge at each Mach number. Additionally, there is little dependence on spanwise location when the results are viewed in this form. It is noted that the spanwise location of zero refers to the fin root, and the spanwise location of one refers to the fin tip.

No further results are shown of computed adiabatic wall temperature for any of the projectile configurations. For the perfect gas applications of this study, it is maintained that the use of a constant free-stream recovery factor r_f= 0.88 is justified for design work. A major point of consideration is the retainment of the same T_{aw} distribution when forming h as when later extracting q during the subsequent heat conduction computations. In this report, all heat transfer coefficients are formed using a constant free-stream recovery r_f= 0.88.

7.2 M735 Projectile - Surface Heat Transfer Coefficient. Figure 8 shows the computed heat transfer coefficient over the M735 projectile forebody and fin leading edge at the two different Mach numbers. On the cone portion of the projectile, the computed heat transfer decreases rapidly with respect to x/d close to the nosetip, and levels off toward what appears to be an asymptotic value further from the nosetip. On the cylinder portion of the projectile, the computed heat transfer distribution is practically constant at each Mach

number, and the difference in the heat transfer coefficient is about 5%. On the fin leading edge, however, the difference in computed heat transfer coefficient between the two Mach numbers is about 30%. Unlike the computed adiabatic wall temperature, the computed heat transfer distribution does not contain numerical spikes.

Figures 9 and 10 show the computed chordwise heat transfer coefficient over the fins at several spanwise locations at the two different Mach numbers. At both Mach numbers, the computed leading edge heat transfer varies only slightly beyond 1/4 span. Downstream from the leading edge, the differences with respect to spanwise location become more apparent. Close to the fin tip, the chordwise heat transfer distribution tends to level off to a constant value downstream from the leading edge. Close to the fin root, the heat transfer distribution passes through a trough which is followed by a smooth rise and fall toward an asymptotic value.

The previous figures show heat transfer results for a constant wall temperature of 294 K. The behavior of the heat transfer coefficient with respect to surface temperature is of interest as well, because the projectile surface temperature increases during the flight. The common engineering approach is to assume that the heat transfer coefficient is constant with respect to wall temperature. It should be noted, however, that a decrease of heat transfer coefficient with respect to wall temperature is predicted by the turbulent flat plate analysis of Van Driest (1951). For hypersonic flow applications, consideration of wall temperature could be important.

Figure 11 shows the effect of body surface (i.e., wall) temperature on the heat transfer coefficient on the forebody and leading edge at $M = 4.36$. Six different surface temperatures are shown, varying from atmospheric temperature to slightly above the adiabatic wall temperature. The surface temperatures have been non-dimensionalized to form a temperature factor, T_f, defined as

$$T_f = \frac{T_w - T_{atm}}{T_{aw} - T_{atm}} \tag{13}$$

in which T_w is the wall temperature, T_{aw} is the adiabatic wall temperature based on a free-stream recovery factor of 0.88, and T_{atm} is the free-stream temperature (taken to be standard atmospheric temperature). When T_w is equal to standard atmospheric temperature, T_f is equal to 0.0; when T_w is equal to the adiabatic wall temperature, T_f is equal to 1.0.

Figure 11 shows the heat transfer coefficient to decrease, by as much as 20%, as the wall temperature increases toward the adiabatic value. Comparing to Figure 8, it can be postulated that the surface temperature effect may be as important as Mach number for an accurate model of in-flight surface heat transfer. The same effect is re-illustrated in Figure 12, where the heat transfer coefficient is plotted as a function of the temperature

factor for several points on the projectile body. The heat transfer coefficient is well behaved and decreases nonlinearly as the surface temperature increases from the atmospheric value toward the adiabatic value.

7.3 M829 Projectile - Surface Heat Transfer Coefficient. As already stated, the heat transfer coefficient reported here is formed using a perfect gas adiabatic wall temperature obtained from Eq. (3), with an assumed value of the free-stream recovery factor $r_f = 0.88$. Figures 13 and 14 show the computed heat transfer coefficient distribution over the M829 projectile forebody and fin leading edge at Mach numbers 4.9 and 4.36, respectively. Also shown is the heat transfer coefficient distribution along the cylinder portion between two adjacent fins; the heat transfer there does not appear to be greatly influenced by the presense of the fins.

Figures 15 and 16 show the computed chordwise distribution of heat transfer coefficient over the fins at several spanwise locations at the two different Mach numbers 4.9 and 4.36, respectively. The leading edge distributions are quite similar between 3/8 and 7/8 span. Downstream from the leading edge, the differences with respect to spanwise location become more apparent.

7.4 F829 (Cone-Cylinder-Flare) - Surface Heat Transfer Coefficient. Results are reported for the F829 cone-cylinder-flare configuration for flare angles varying from 0° to 20° in increments of 4°. The PNS solutions were marched over the flare without the use of a fillet for flare angles to 12°. A fillet of approximate length 0.1 calibers was added to the cases with larger flare angles.

Figures 17 through 20 show the computed heat transfer coefficient for the F829 configuration at Mach numbers 11.8, 8.8, 5.9, and 4.4, respectively. The flare angle is plotted as an additional parameter in each figure. For flare angles to 8°, the computed heat transfer coefficient barely reaches a peak value on the flare. For higher flare angles, the heat transfer coefficient reaches a peak value on the flare and decreases somewhat before the flow reaches the aft end. At each Mach number, the location of peak heat transfer on the flare moves forward with increasing flare angle. Also, for a constant flare angle, the location of peak heat transfer moves rearward with the combination of increasing Mach number and increasing Reynolds number that represents atmospheric sea-level conditions.

An interesting comparison of heat transfer coefficient can be made between Figure 14 (M829) and Figure 20 (F829). The free-stream Mach number of these two cases is within 0.04, and the sweeps of the fin and flare are within 0.25°. The peak leading edge heat transfer

coefficient of the M829 is about 60% greater than the peak flare heat transfer coefficient of the F829 with a 20° flare angle.

8. CONCLUSION

Viscous computational fluid dynamics (CFD) predictions have been presented of the surface heat transfer characteristics of three kinetic energy (KE) projectile configurations. Two of the configurations are fielded, fin-stabilized KE projectiles (M735 and M829). The third is a cone-cylinder flare (F829) configuration which is a conceptual hypervelocity projectile configuration formed by replacing the fins of the M829 with a conical flare of various sweep angles. Results were presented of the perfect gas adiabatic wall temperature and surface heat transfer coefficient, obtained using a parabolized Navier-Stokes (PNS) computational technique.

The CFD predictions of adiabatic wall temperature at Mach 4.36 show variations of only a few percent over the entire projectile surface. This demonstrates that a reasonable engineering approximation can be made of the perfect gas adiabatic wall temperature by employing a free-stream recovery factor of 0.86 to 0.89. Based on this finding, a free-stream recovery factor of 0.88 was assumed throughout the study, and the surface heat transfer coefficient was formed using such a convention.

The predictions of surface heat transfer coefficient show substantial differences in behavior over the various surfaces of the projectiles. For both the M735 and M829, the heat transfer coefficient on the cylinder is computed to decrease by only about 5% between the velocities at launch and 2 seconds into flight (a range of about 3 km). On the other hand, the heat transfer coefficient on the fin leading edge is computed to decrease by about 30% in this same time frame.

The computed chordwise distributions of heat transfer rate on the fins of both configurations show dependence on spanwise location, but the importance of these differences in the transient thermal response of the fins is unknown. Computations for wall temperatures greater than the atmospheric temperature show that the heat transfer coefficient decreases noticeably as the surface temperature of the projectile increases toward the adiabatic wall temperature.

The heat transfer coefficient for the F829 cone-cylinder-flare configuration was presented for flare angles to 20°. Flare angles less than 8° do not show a significant peak in heat transfer on the flare itself. Higher flare angles show the heat transfer to reach a peak on the flare and decrease somewhat before the flow reaches the aft end. The location of this peak is shown to depend on the flare angle, as well as the combination of Mach number and Reynolds number that represents atmospheric sea-level free-flight conditions. At a Mach number of approximately 4.4, the peak leading edge heat transfer rate of the M829 is about 60% greater than the peak flare heat transfer of the F829 with a 20° flare.

The computed heat transfer characteristics reported here are important because they provide a necessary boundary condition for subsequent heat conduction computations, in which the transient in-flight thermal response is simulated. The incorporation of CFD heat transfer boundary conditions into such simulations is ongoing. The computation and assessment of real gas and blunt nosetip effects on the heat transfer characteristics is also being pursued.

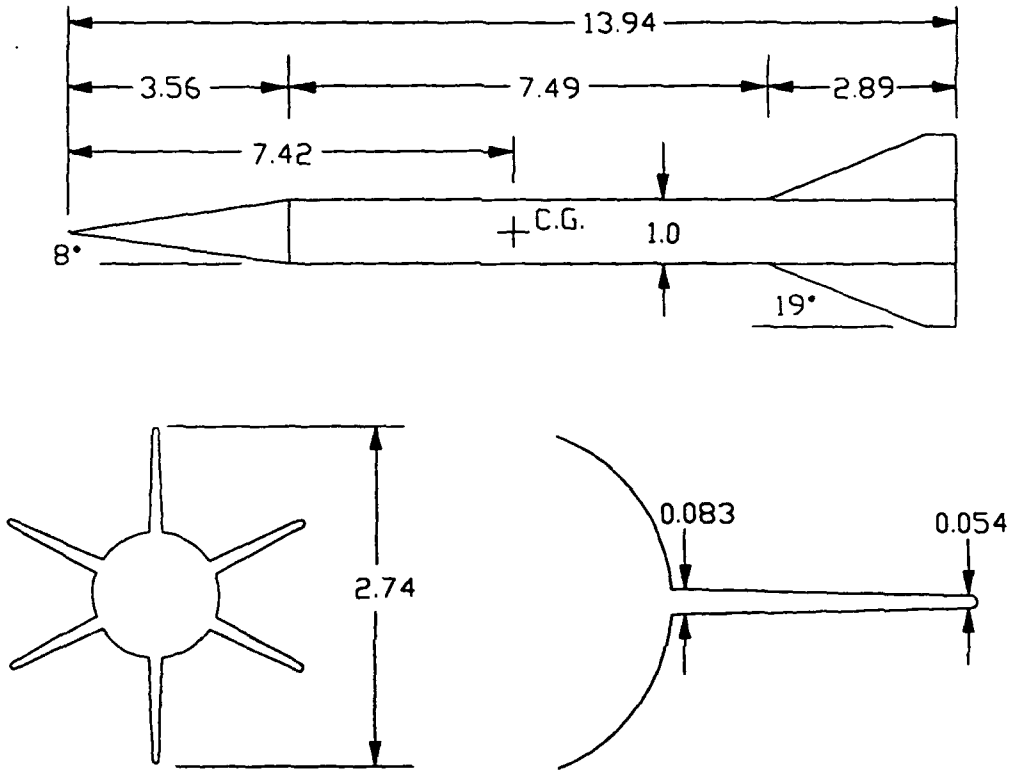

Figure 1. Schematic of M735 Projectile Model

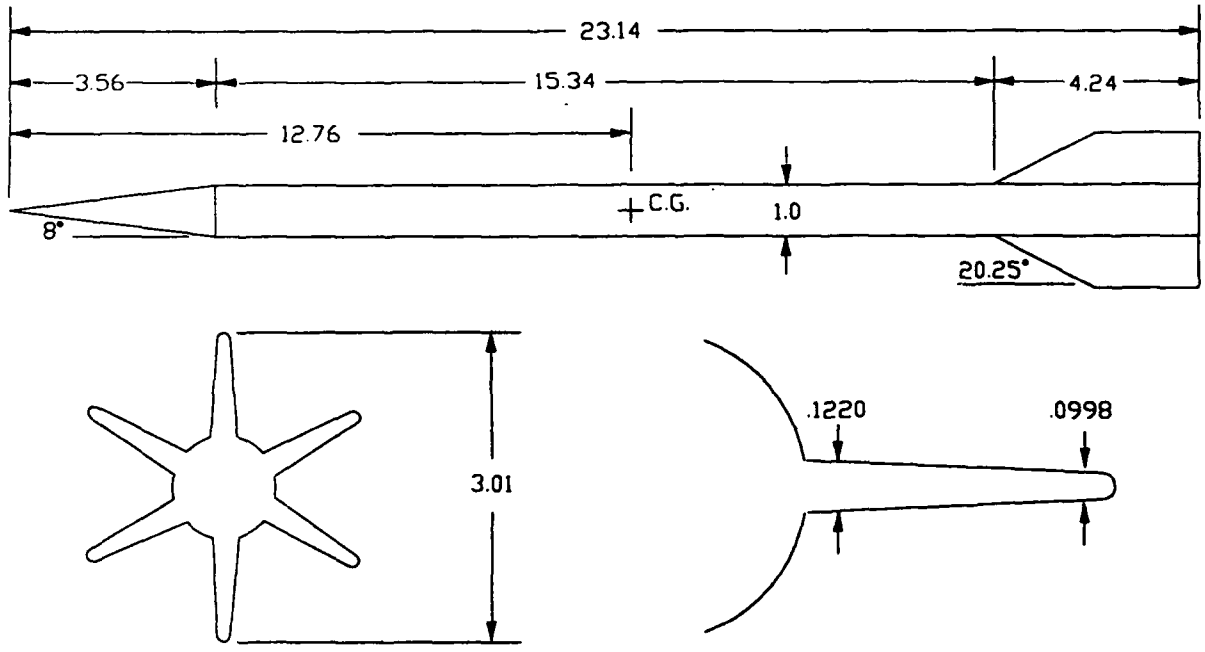

Figure 2. Schematic of M829 Projectile Model

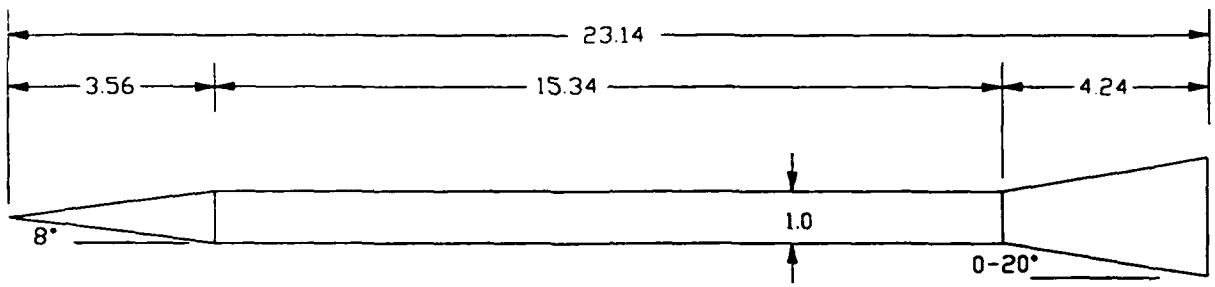

All Dimensions in Calibers (One Caliber=27.05mm)

Figure 3. Schematic of F829 Cone-Cylinder-Flare Model

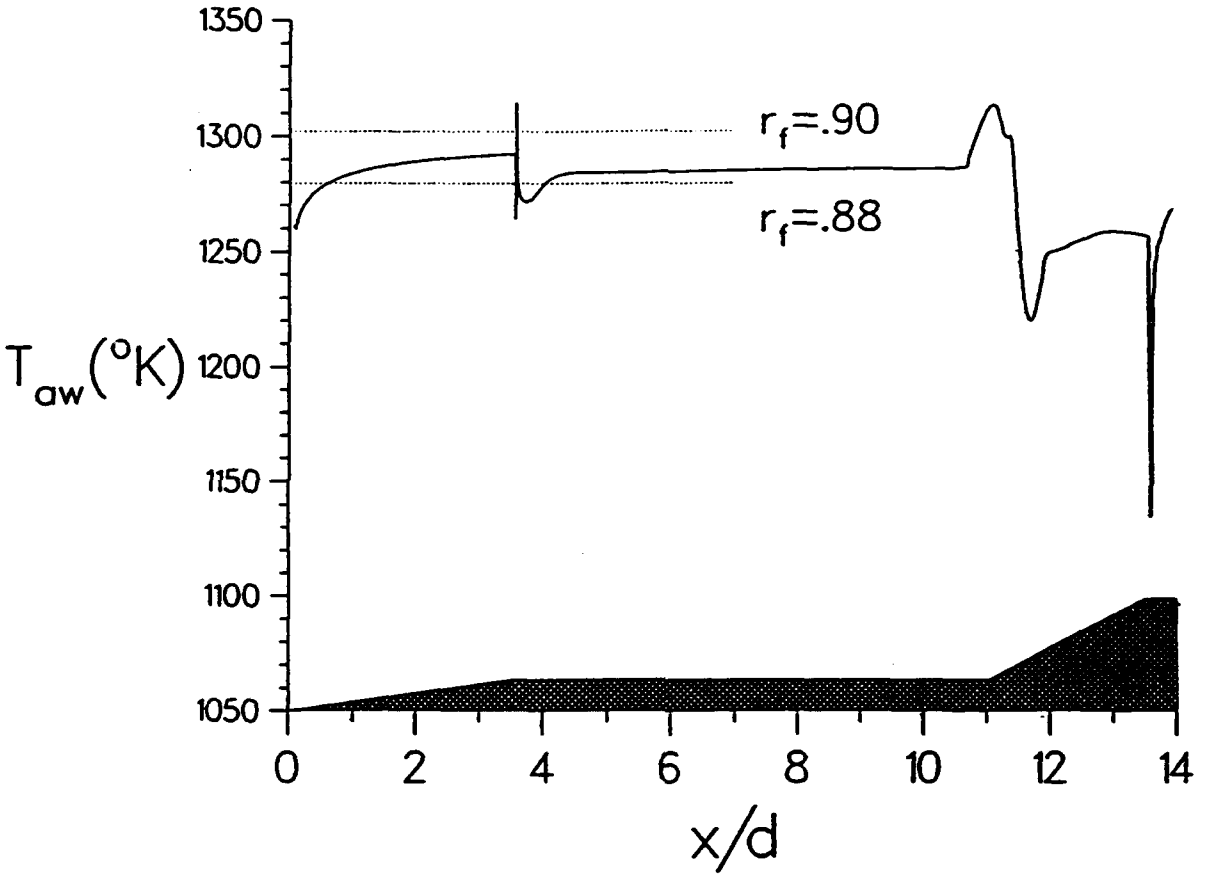

Figure 4. Adiabatic Wall Temperature Over M735 Forebody and Fin Leading Edge, M=4.36

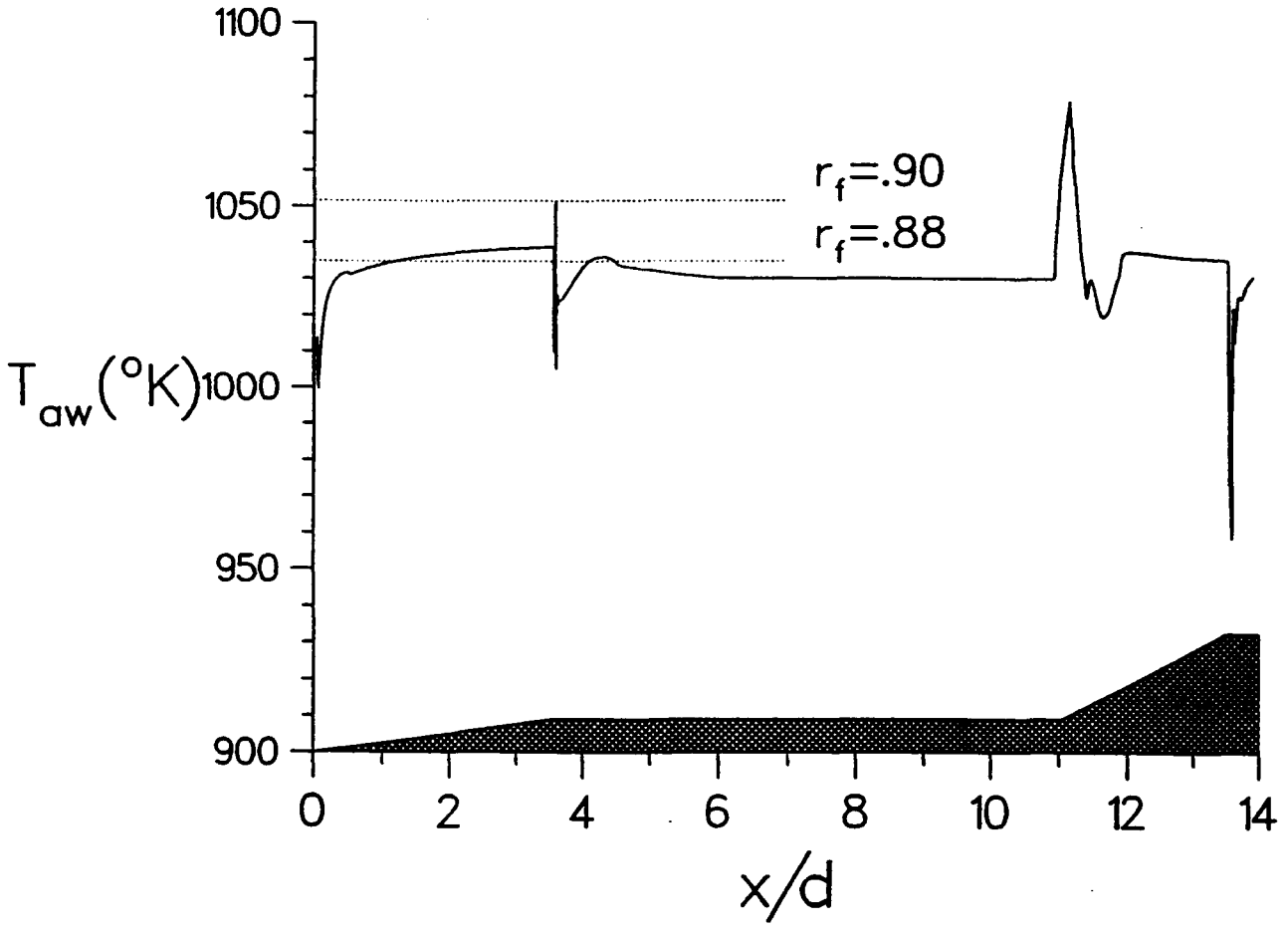

Figure 5. Adiabatic Wall Temperature Over M735 Forebody and Fin Leading Edge, M=3.78

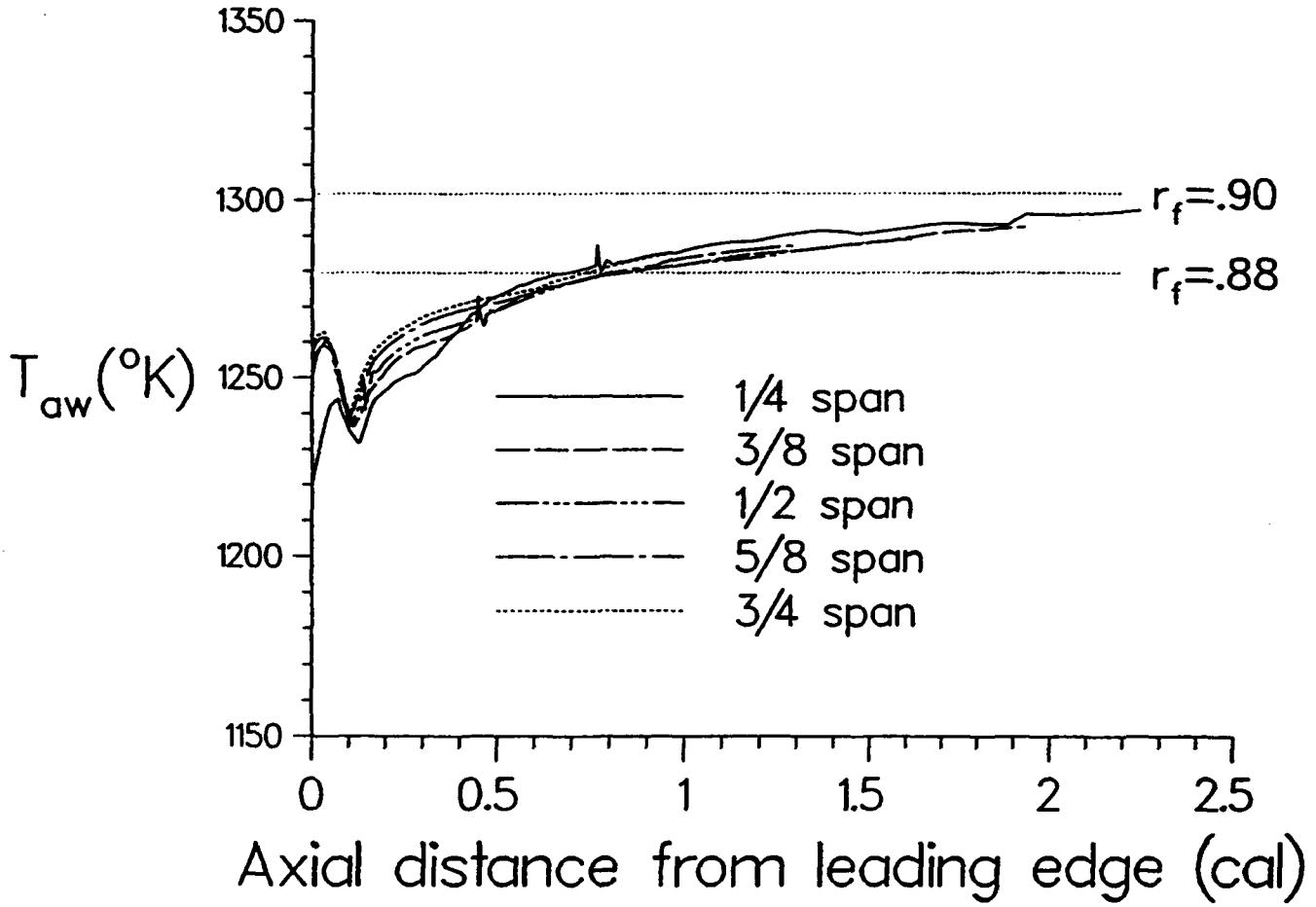

Figure 6. Adiabatic Wall Temperature Over M735 Fin, M=4.36

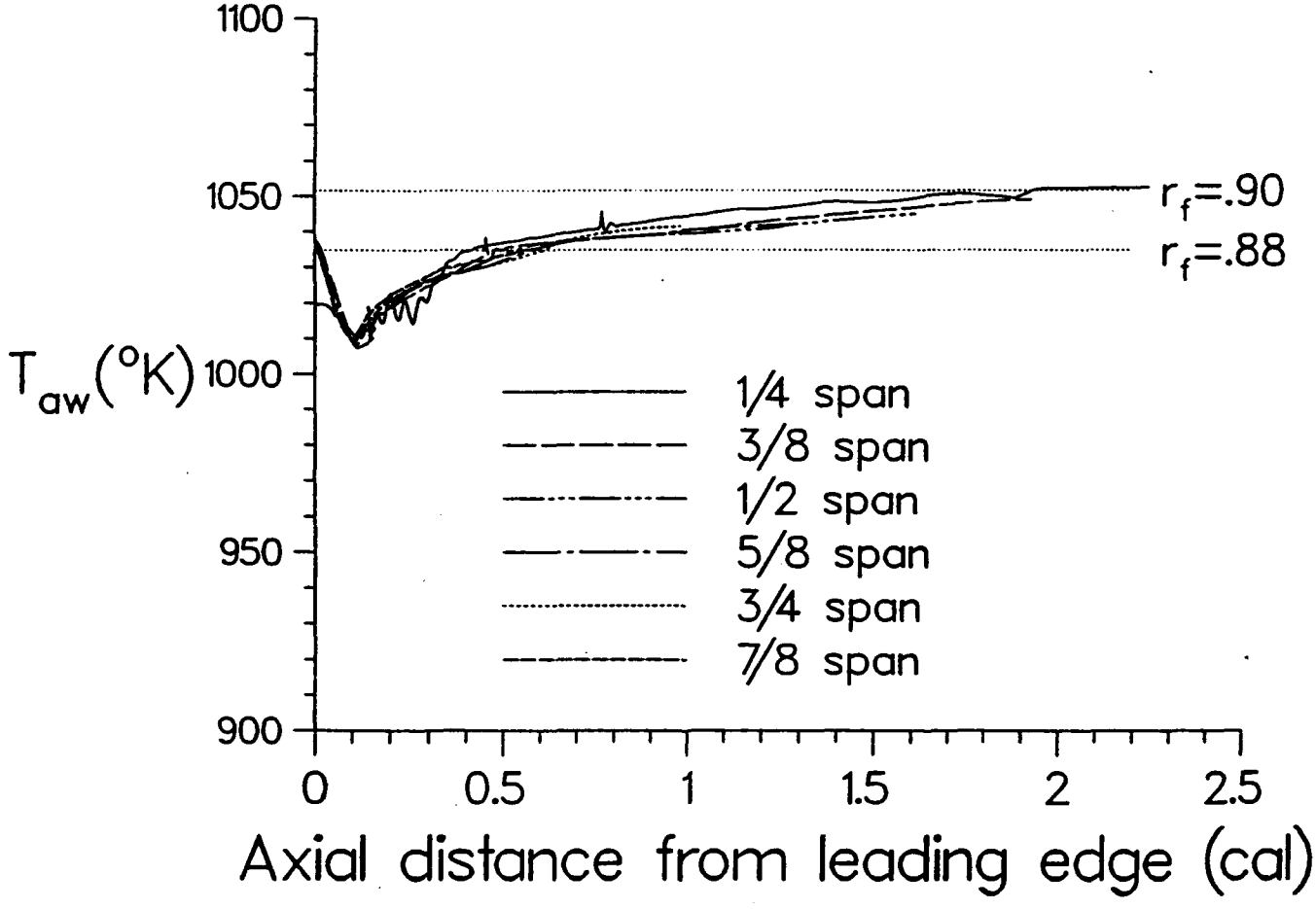

Figure 7. Adiabatic Wall Temperature Over M735 Fin, M=3.78

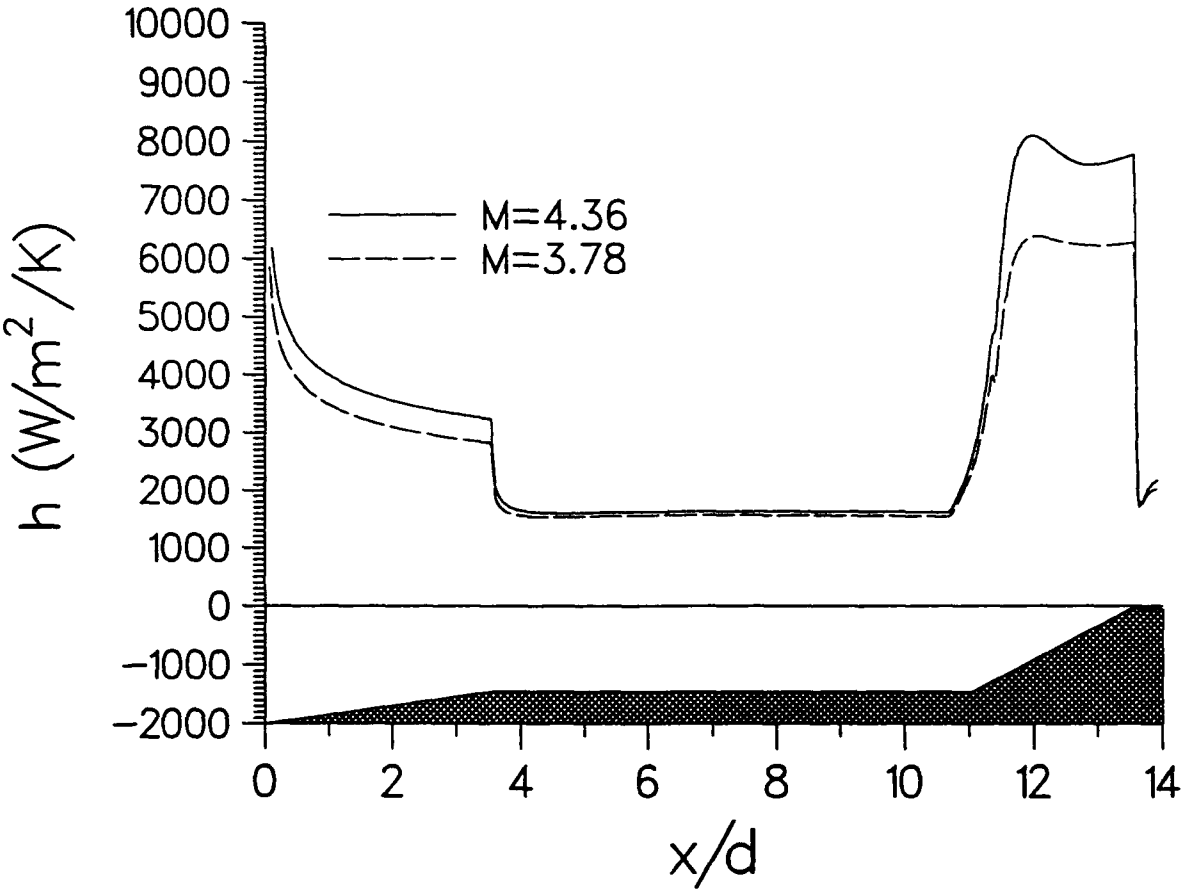

Figure 8. Surface Heat Transfer Coefficient Over M735 Forebody and Fin Leading Edge, M=4.36 and M=3.78

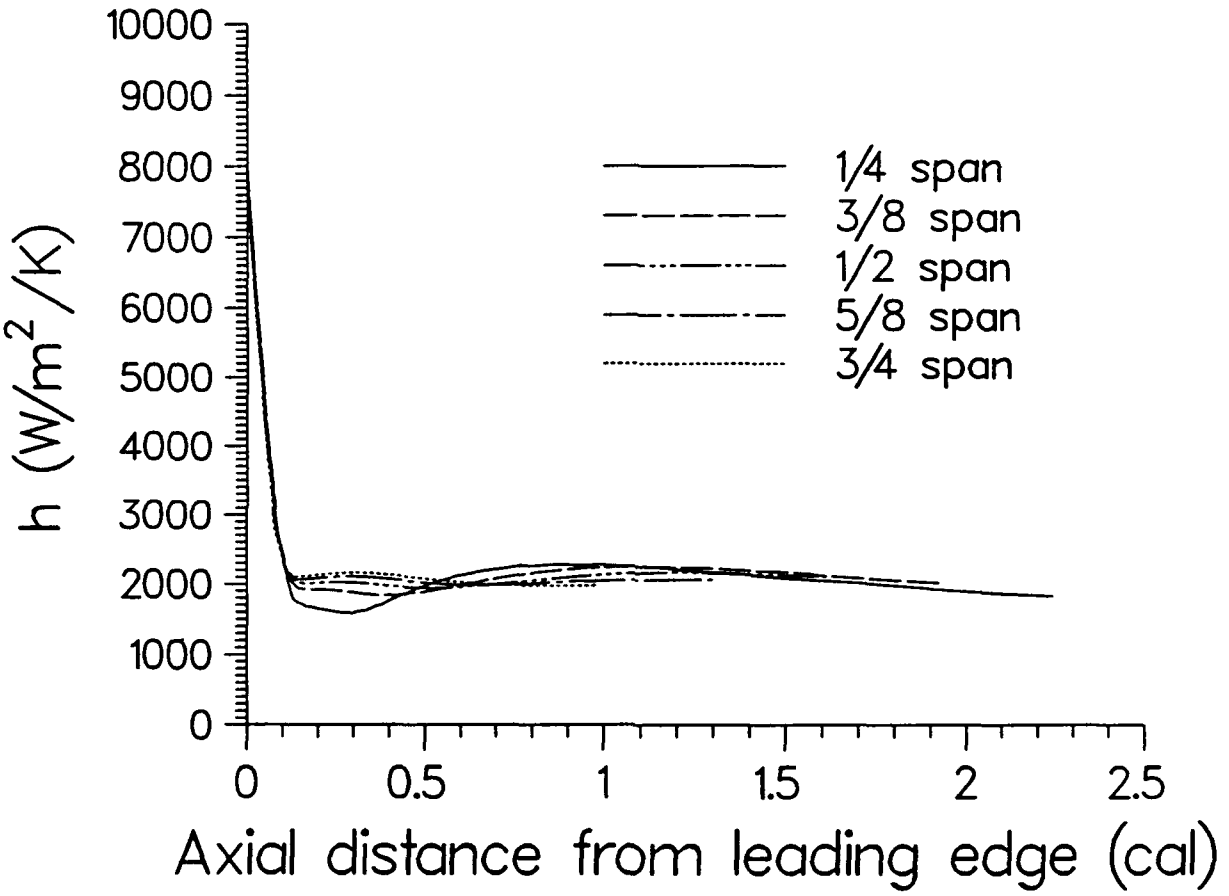

Figure 9. Surface Heat Transfer Coefficient Over M735 Fin, M=4.36

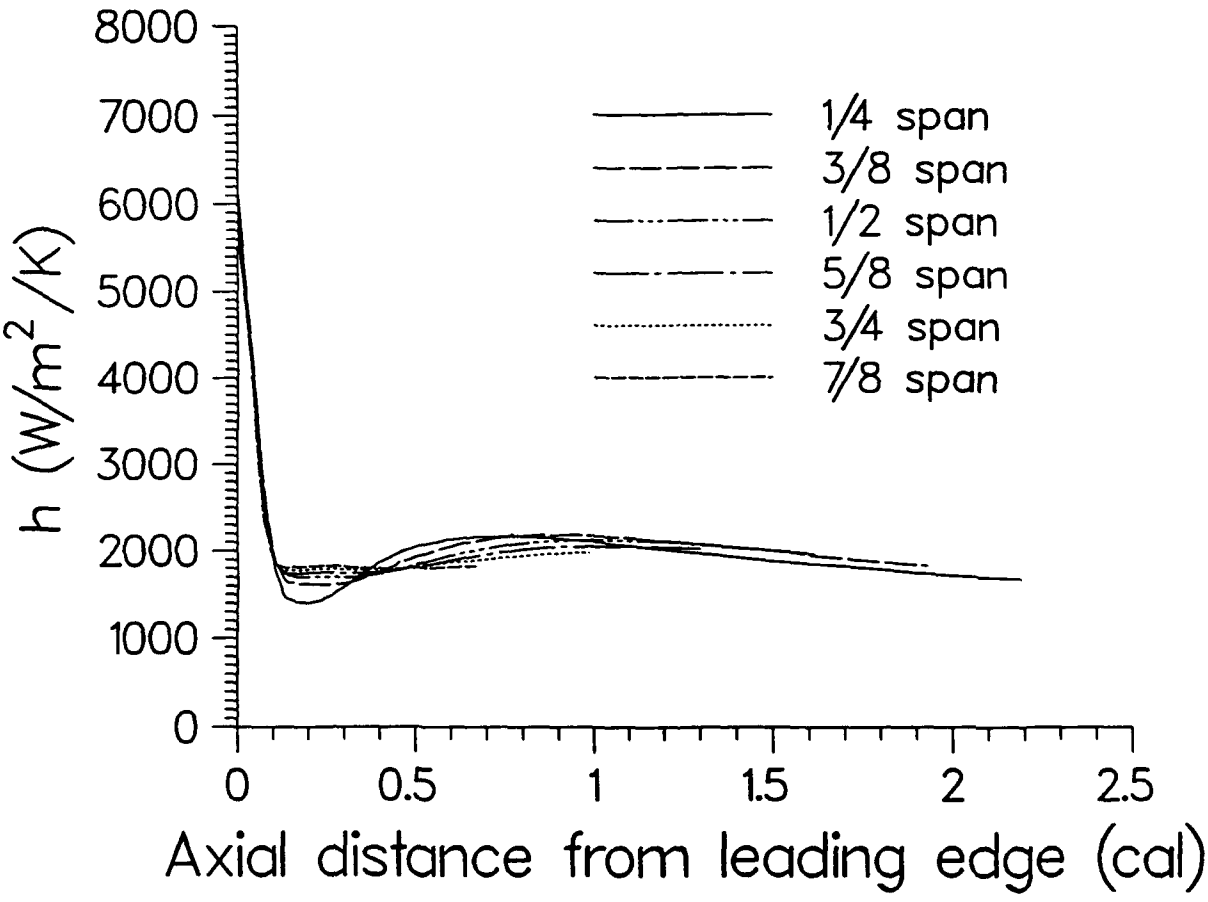

Figure 10. Surface Heat Transfer Coefficient Over M735 Fin, M=3.78

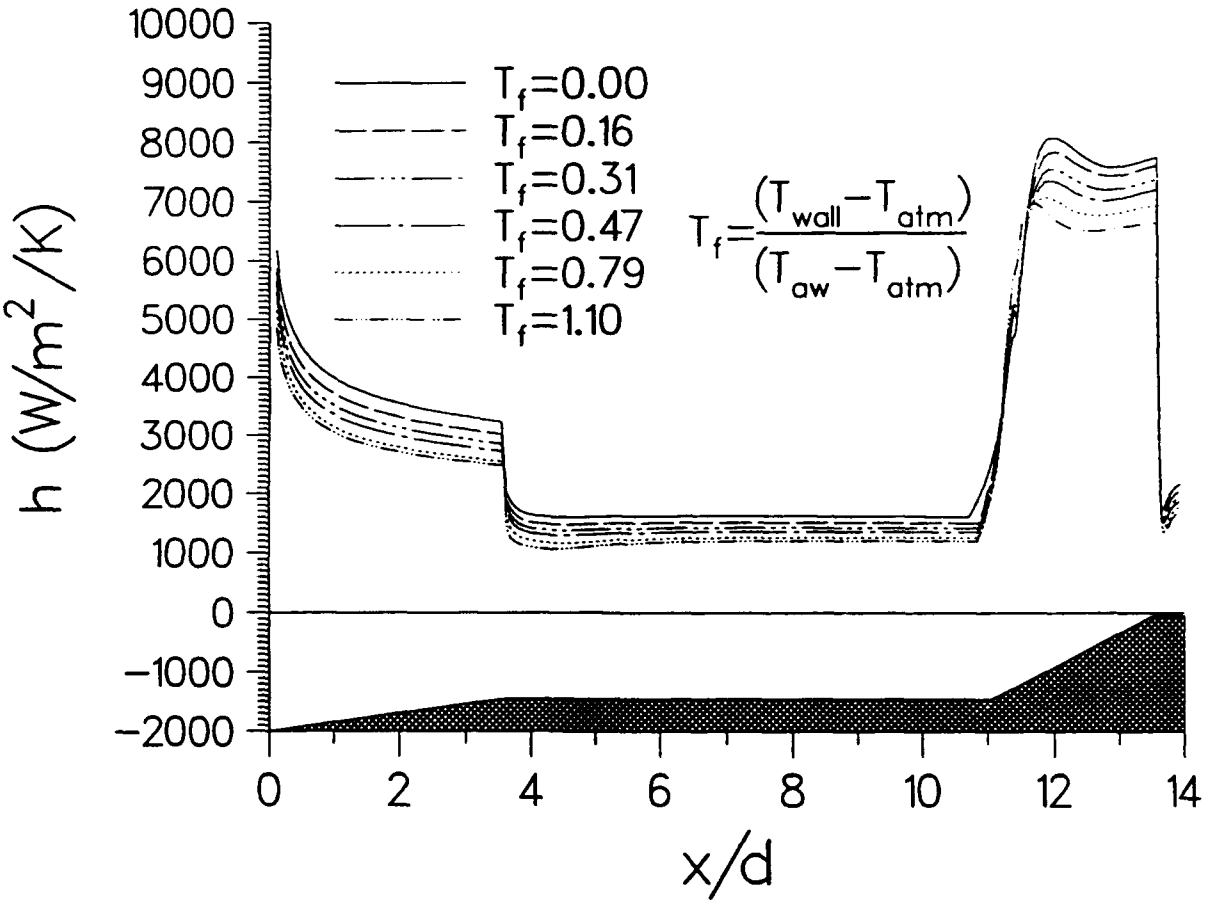

Figure 11. Effect of Surface Temperature on Computed Surface Heat Transfer Coefficient Over M735 Forebody and Fin Leading Edge, M=4.36

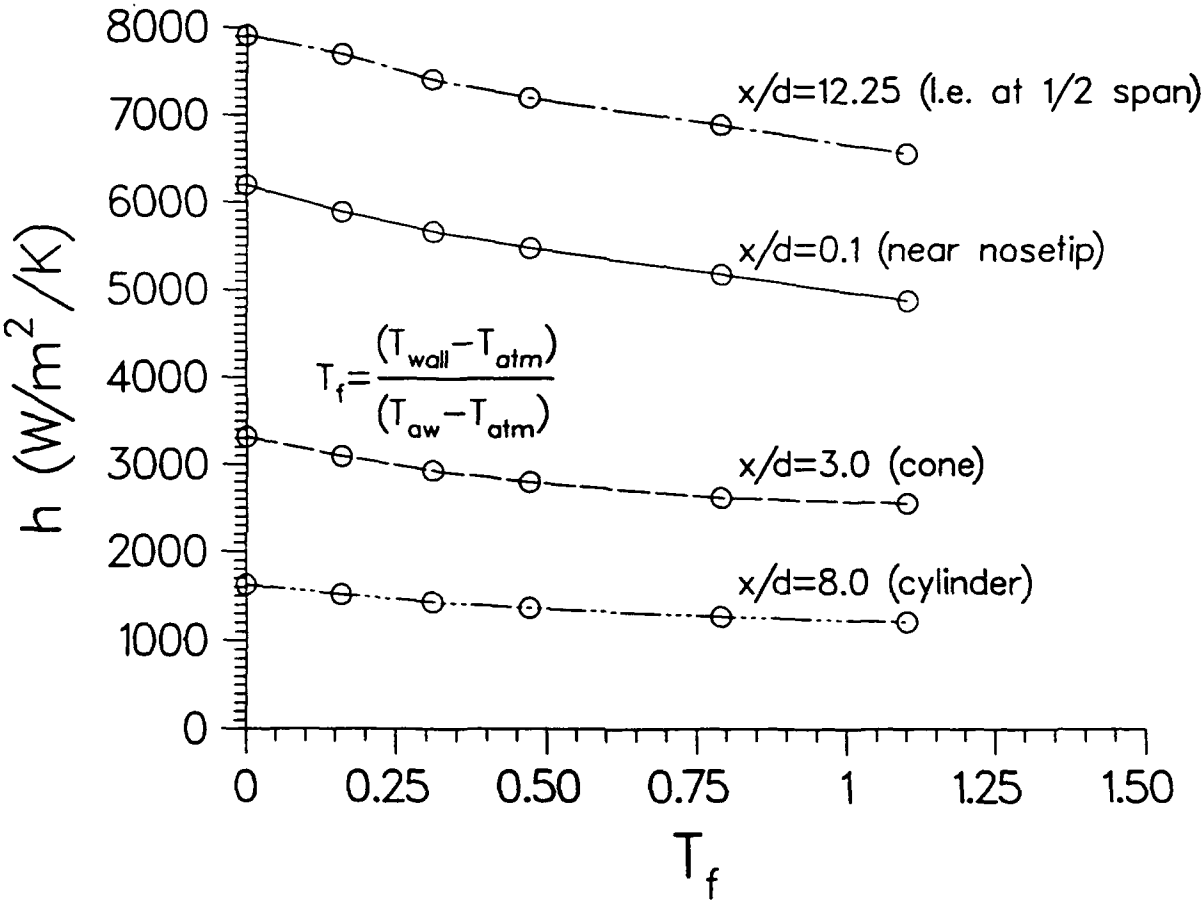

Figure 12. Surface Heat Transfer Coefficient vs. Wall Temperature at Several Locations on M735, M=4.36

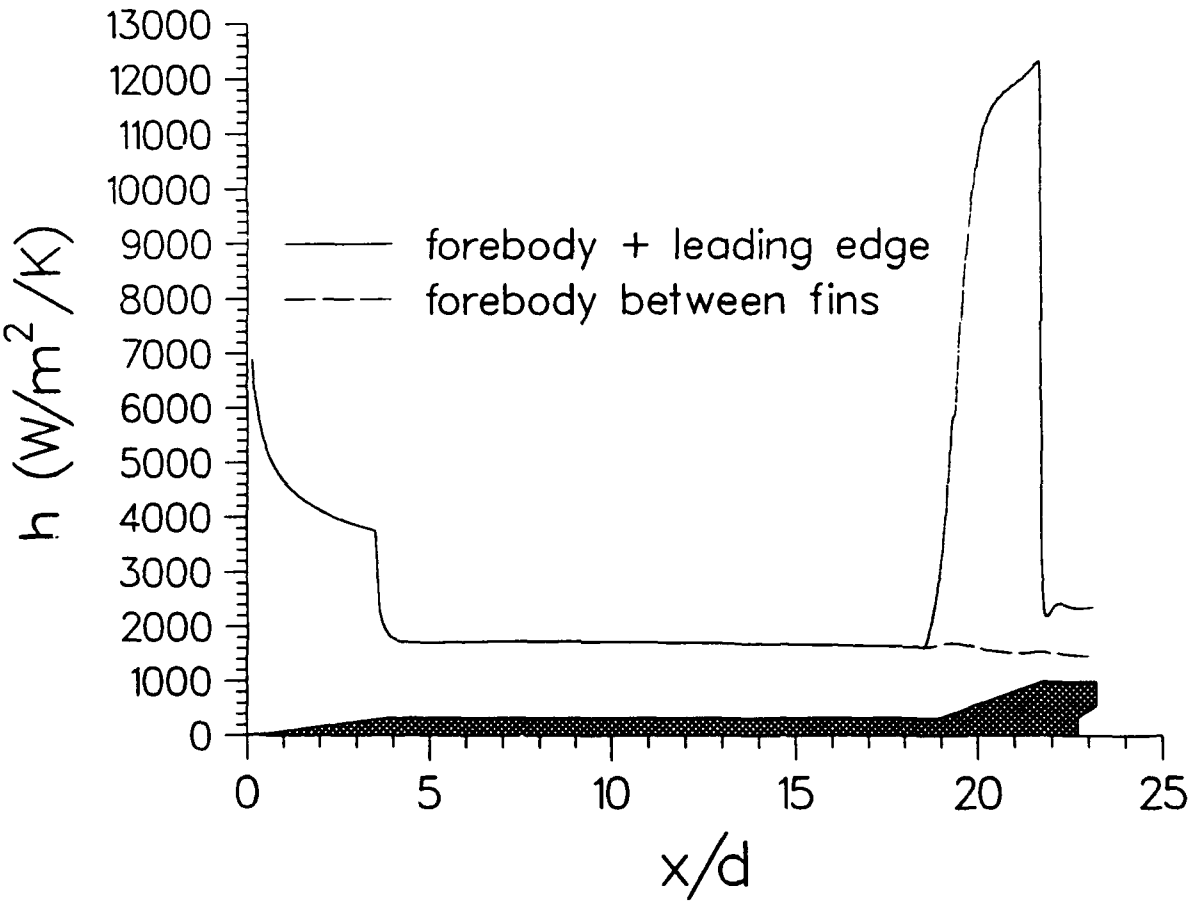

Figure 13. Surface Heat Transfer Coefficient Over M829 Forebody and Fin Leading Edge, M=4.9

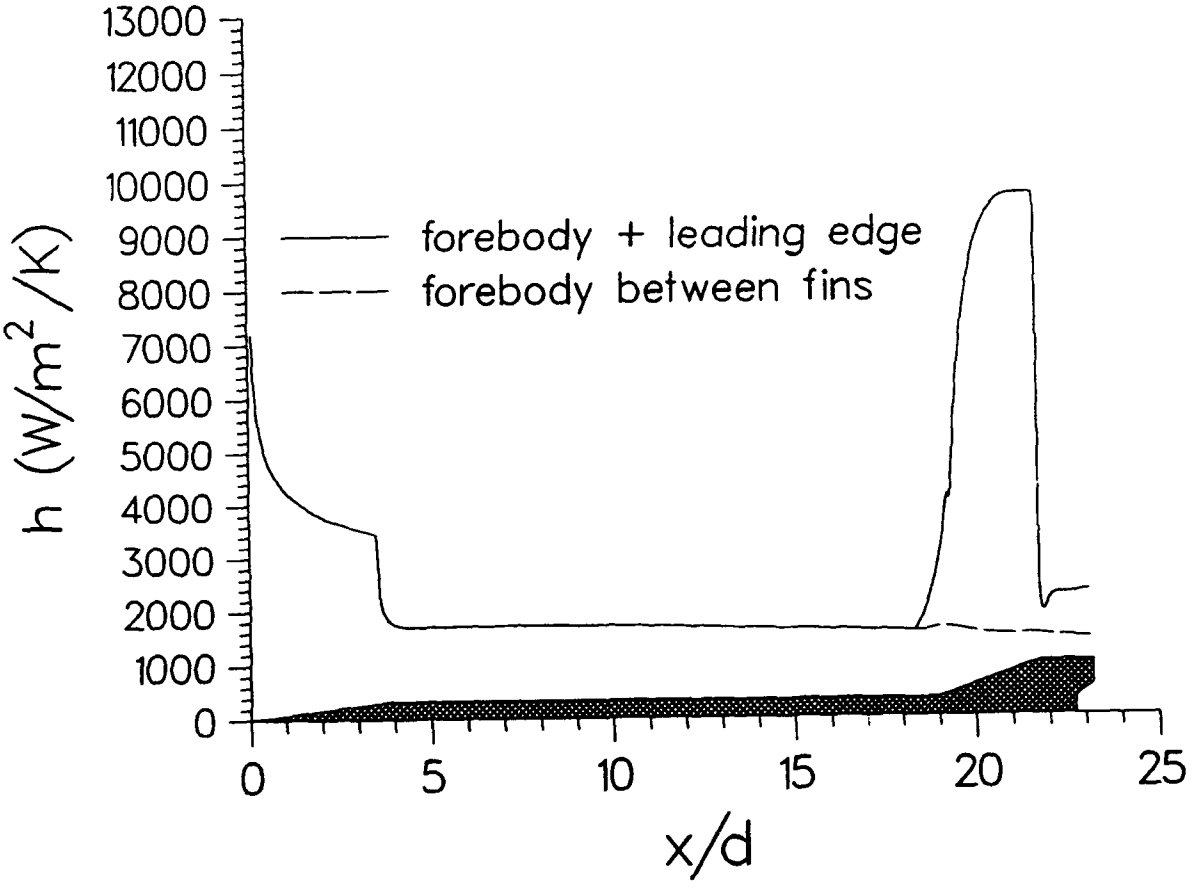

Figure 14. Surface Heat Transfer Coefficient Over M829 Forebody and Fin Leading Edge, M=4.36

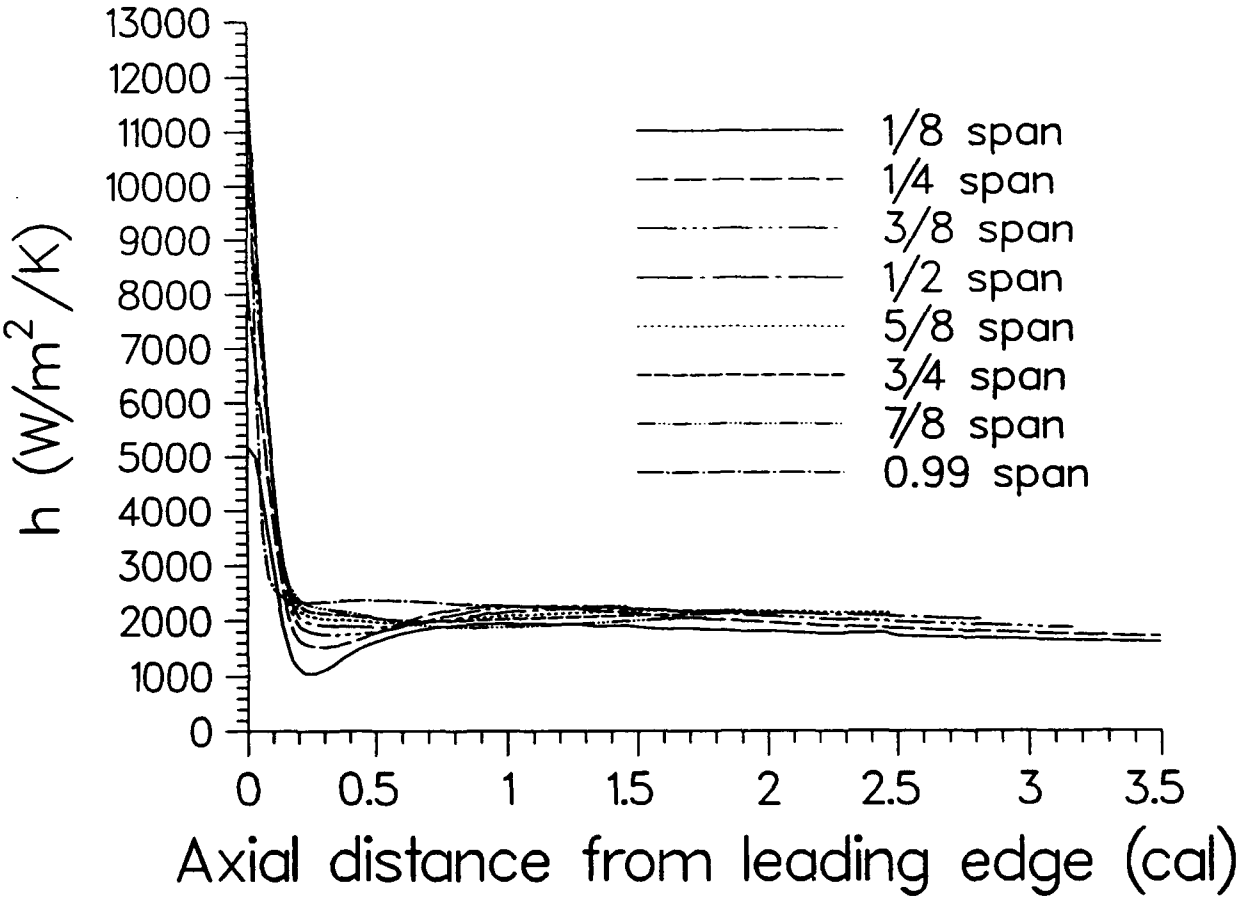

Figure 15. Surface Heat Transfer Coefficient Over M829 Fin, M=4.9

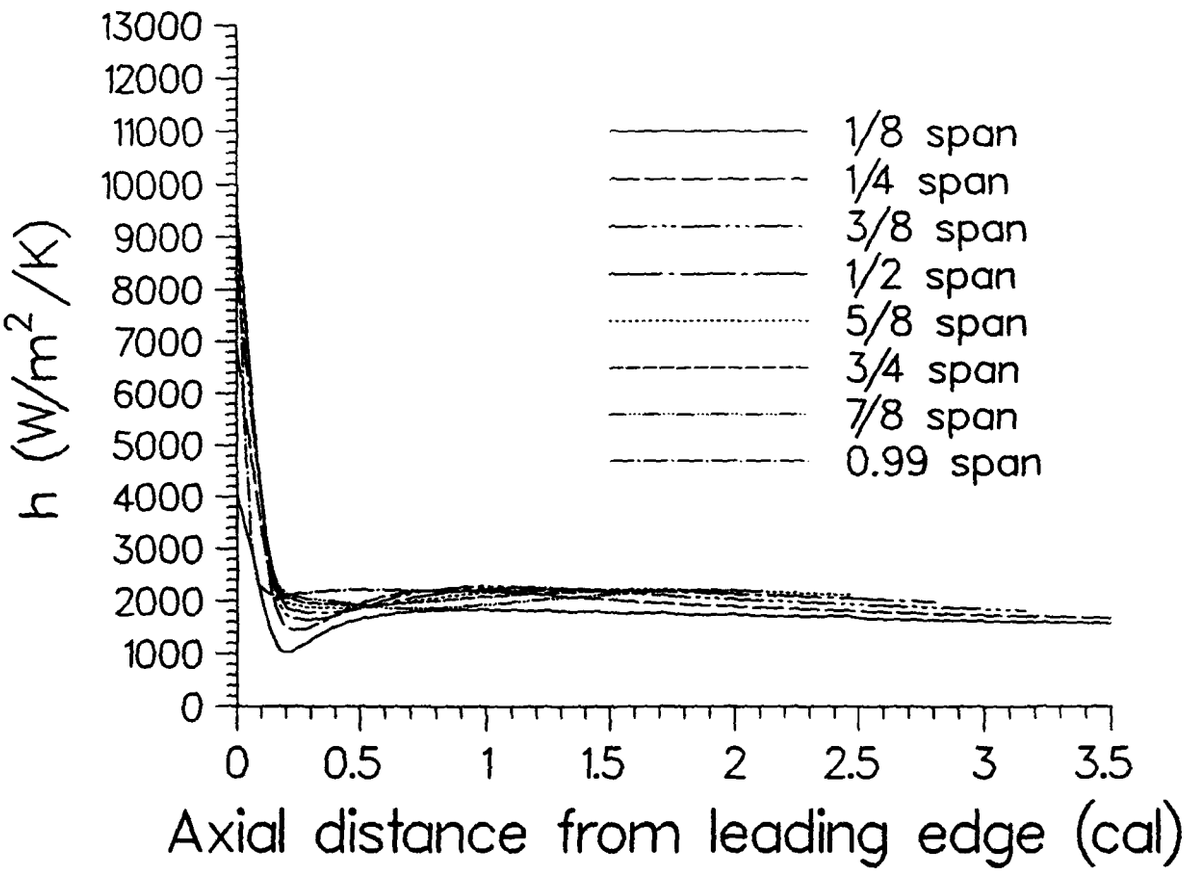

Figure 16. Surface Heat Transfer Coefficient Over M829 Fin, M=4.36

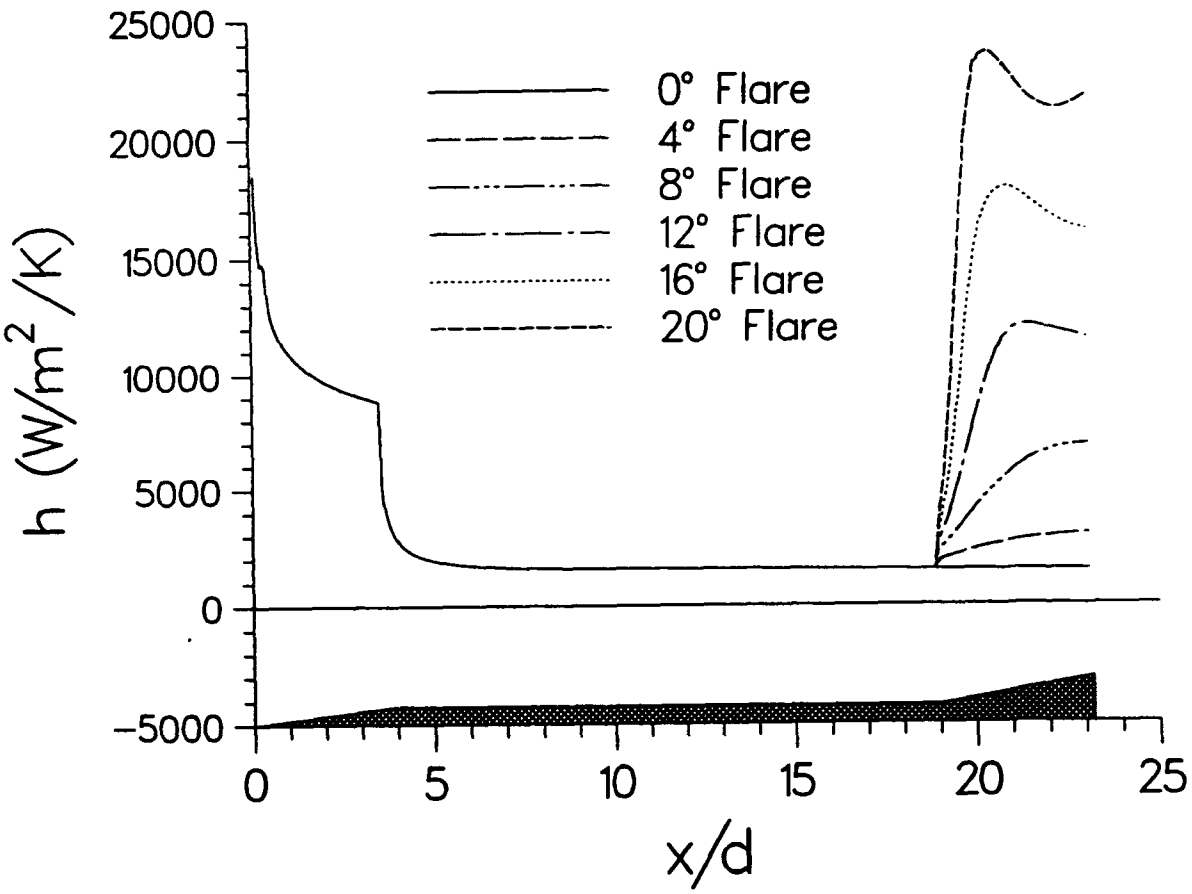

Figure 17. Surface Heat Transfer Coefficient Over F829, M=11.8

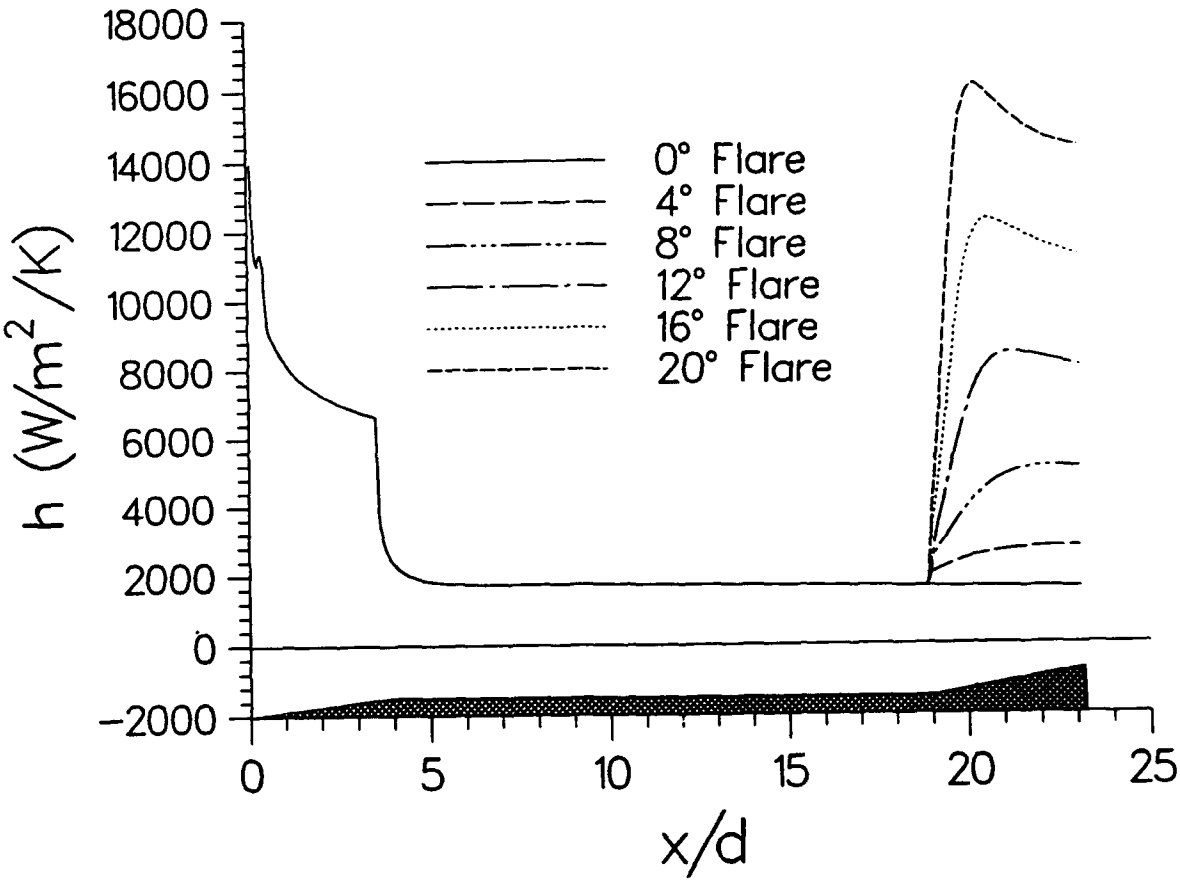

Figure 18. Surface Heat Transfer Coefficient Over F829, M=8.8

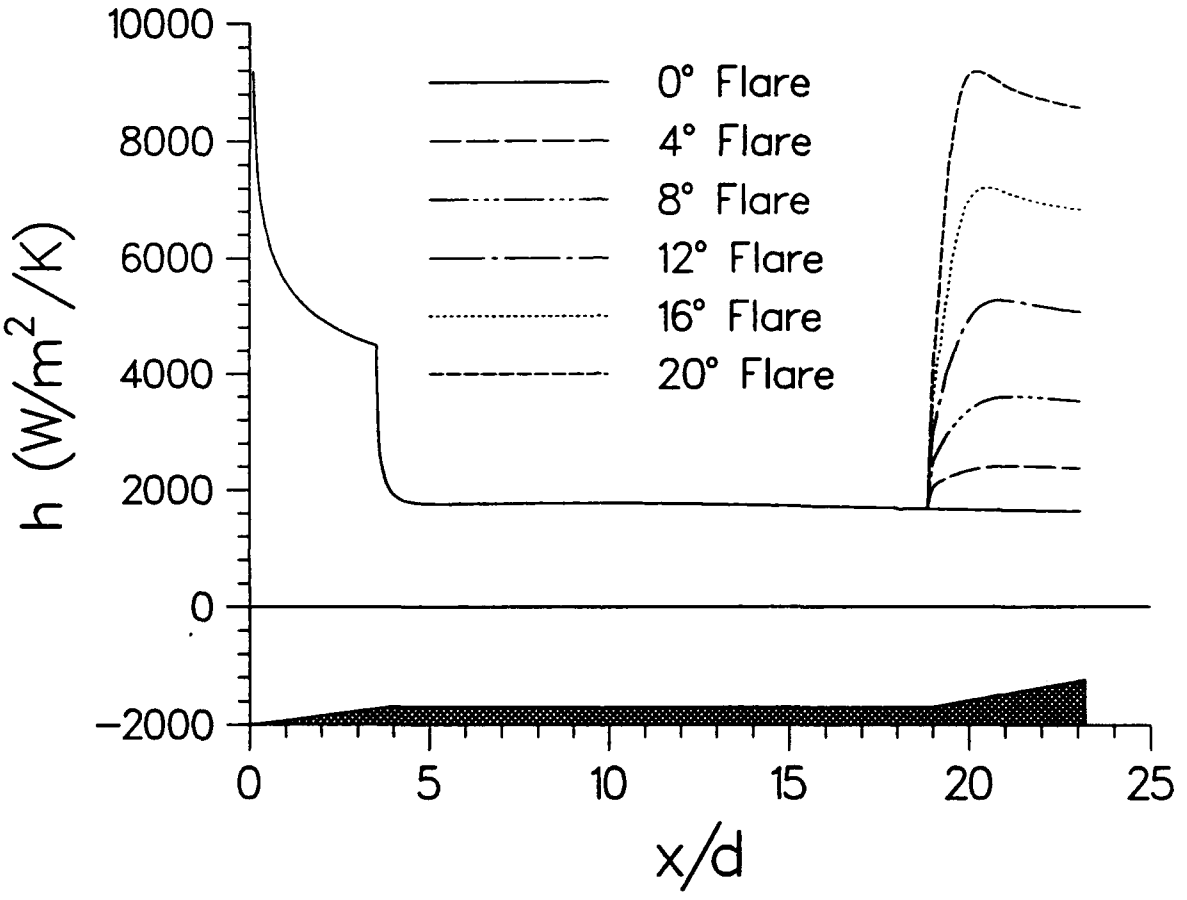

Figure 19. Surface Heat Transfer Coefficient Over F829, M=5.9

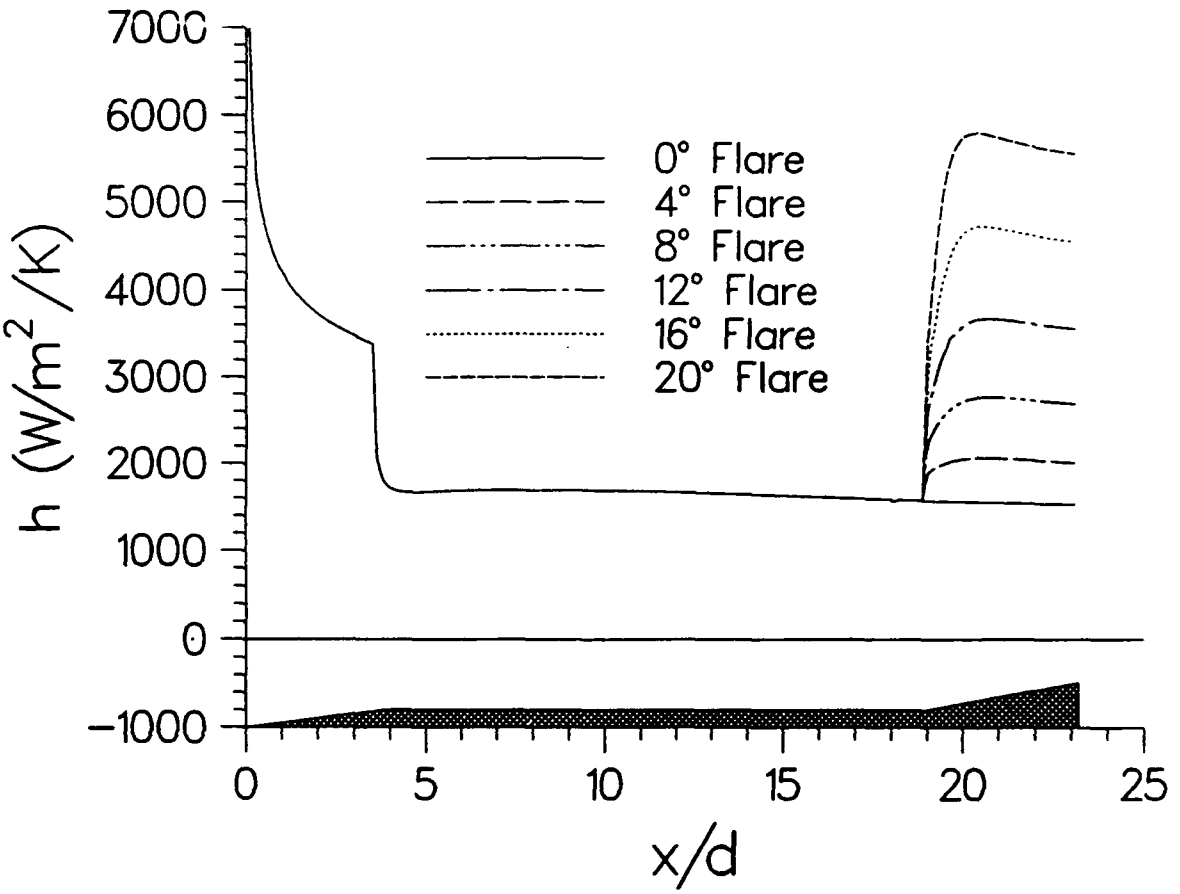

Figure 20. Surface Heat Transfer Coefficient Over F829, M=4.4

9. REFERENCES

Ackermann, G. "Plate Thermometer in High Velocity Flow with Turbulent Boundary Layer," Forshung auf Gebiete des Ingenieurwesens, Vol. 13, p.226, 1942.

Balakrishnan, A., and P. Weinacht. "Improvements to Flowfield Codes for Predicting Accurate Heat Transfer Rates," AIAA Paper No. 86-1286, June 1986.

Baldwin, B.S., and H. Lomax. "Thin-Layer Approximation and Algebraic Model for Separated Turbulent Flows," AIAA Paper No. 78-0257, January 1978.

Beam, R., and R.F. Warming. "An Implicit Factored Scheme for the Compressible Navier-Stokes Equations," AIAA Journal, Vol. 16, No. 4, pp. 393-402, 1978.

Dwyer, H.A., R.J. Kee, and B.R. Sanders. "Adaptive Grid Method for Problems in Fluid Mechanics and Heat Transfer," AIAA Journal, Vol. 18, No. 10, pp. 1205-1212, October 1980.

Eber, G.R. "Recent Investigations of Temperature Recovery and Heat Transmission on Cones and Cylinders in Axial Flow in the NOL Aeroballistics Wind Tunnel," Journal of Aeronautical Science, Vol. 19, pp. 1-6, 1952.

Emmons, H.W., and J.G. Brainard. "Effect of Variable Viscosity on Boundary Layers, with a Discussion of Drag Measurements," Journal of Applied Mechanics, Vol. 64, p. 105, 1942.

Evvard, J.C., M. Tucker, and W.C. Burgess. "Statistical Study of Transition Point Fluctuations in Supersonic Flow," NACA TN 3100, 1954.

Guidos, B.J., P.Weinacht, and D.S. Dolling, "Comparison of Navier-Stokes Computation and Experiment for Pointed, Spherical, and Flat Tipped Shell at Mach 2.95," BRL-TR-3076, U.S. Army Ballistic Research Laboratory, Aberdeen Proving Ground, Maryland, January 1990. (AD A218749)

Kobayashi, W.S. "Aerodynamic Heating Computations for Projectiles - Volume I: In-depth Heat Conduction Modifications to the ABRES Shape Change Code (BRLASCC)," Contract Report ARBRL-CR-00527, U.S. Army Ballistic Research Laboratory, Aberdeen Proving Ground, Maryland, June 1984. (AD A143252)

Kutler, P., J.A. Pedelty, and T.H. Pulliam. "Supersonic Flow over Three-Dimensional Ablated Nosetips Using an Unsteady Implicit Numerical Procedure," AIAA Paper No. 80-0063, January 1980.

Nicolet, W.E., and G.R. Srinivasan. "Assessment of Real Gas Effects on the Prediction of the Aerodynamics of High Velocity Army Shells," Thermal Sciences Report 82-02, Thermal Sciences, Inc., 1982.

Nusca, M.J. "Supersonic/Hypersonic Aerodynamics and Heat Transfer for Projectile Design Using Viscous-Inviscid Interaction," BRL-TR-3119, U.S. Army Ballistic Research Laboratory, Aberdeen Proving Ground, Maryland, June 1990. (AD A224354)

Rai, M.M., and D.S. Chaussee. "New Implicit Boundary Procedures: Theory and Applications," AIAA Paper No. 83-0123, January 1983.

Rai, M.M., D.S. Chaussee, and Y.M. Rizk. "Calculation of Viscous Supersonic Flows Over Finned Bodies," AIAA Paper No. 83-1667, July 1983.

Schlichting, H. Boundary Layer Theory, Fourth Edition, McGraw-Hill Book Company, Inc., 1962.

Schiff, L.B., and J.L. Steger. "Numerical Simulation of Steady Supersonic Flow," AIAA Paper No. 79-0130, January 1979.

Schiff, L.B., and W.B. Sturek. "Numerical Simulation of Steady Supersonic Flow over an Ogive Cylinder Boattail Body," ARBRL-TR-02363, U.S. Army Ballistic Research Laboratory, Aberdeen Proving Ground, Maryland, September 1981. (AD 106060)

Strawn, R.C., and W.S. Kobayashi. "Aerodynamic Heating Computations for Projectiles - Vol. II: Swept Wing Calculations Using the Planar Version of the ABRES Shape Change Code (PLNRASCC)," Contract Report ARBRL-CR-00528, U.S. Army Ballistic Research Laboratory/ AARADCOM, Aberdeen Proving Ground, Maryland, June 1984. (AD A143253)

Sturek, F.D., W.B. Sturek, and E.N. Ferry Jr. "A Computational Study of the Effectiveness of Coating Materials for KE Projectile Fins Subjected to the Combined Effects of Inbore and Aerodynamic Heating," BRL-MR-3831, U.S. Army Ballistic Research Laboratory, Aberdeen Proving Ground, Maryland, April 1990.(AD A222595)

Sturek, W.B., H.A. Dwyer, and E.N. Ferry Jr. "Prediction of In-Bore and Aerodynamic Heating of KE Projectile Fins," BRL-MR-3852, U.S. Army Ballistic Research Laboratory, Aberdeen Proving Ground, Maryland, August 1990.(AD 226402)

Sturek, W.B., L.D. Kayser, D.C. Mylin, and H. Hudgins. "Computational Modeling of Aerodynamic Heating for XM797 Nose Cap Configurations," ARBRL-TR-02523, U.S. Army Ballistic Research Laboratory/AARADCOM, Aberdeen PRoving Ground, Maryland, September 1983. (AD A133684)

Sturek, W.B., L.D. Kayser, and P. Weinacht. "Computational Study of Swept-Fin Aerodynamic Heating for the 105mm M774," ARBRL-MR-03315, U.S. Army Ballistic Research Laboratory/ AARADCOM, Aberden Proving Ground, Maryland, October 1983.(AD A134992)

Sturek, W.B., and L.B. Schiff. "Computations of the Magnus Effect for Slender Bodies in Supersonic Flow," ARBRL-TR-02384, U.S. Army Ballistic Research Laboratory, Aberdeen Proving Ground, Maryland, December 1981. (AD 110016)

Suchsland, K.E. "Aerothermal Assessment of Projectiles Using the ABRES Shape Change Code (ASCC)," Contract Report ARBRL-CR-00462, U.S. Army Ballistic Research Laboratory/ AARADCOM, Aberdeen Proving Ground, Maryland, August 1981. (AD B059855)

Truitt, R.W. Fundamentals of Aerodynamic Heating, The Ronald Press Company, 1960.

Van Driest, E.R. "Turbulent Boundary Layer in Compressible Fluids," Journal of the Aeronautical Sciences, Vol. 18, No. 3, pp. 145-160, March 1951.

Weinacht, P., B.J. Guidos, L.D. Kayser, and W.B. Sturek. "PNS Computations for Spinning and Fin-Stabilized Projectiles at Supersonic Speeds," ARBRL-MR-3464, U.S. Army Ballistic Research Laboratory, Aberdeen Proving Ground, Maryland, September 1985. (AD A160393)

Weinacht, P., B.J. Guidos, W.B. Sturek, and B.A. Hodes. "PNS Computations for Spinning Shell at Moderate Angles of Attack and for Long L/D Finned Projectiles," BRL-MR-3522, U.S. Army Ballistic Research Laboratory, Aberdeen Proving Ground, Maryland, June 1986. (AD 169531)

Weinacht, P., and W.B. Sturek. "Computation of the Roll Characteristics of Finned Projectiles," BRL-TR-2931, U.S. Army Ballistic Research Laboratory, Aberdeen Proving Ground, Maryland, June 1988. (AD 197875)

Weinacht, P., and W.B. Sturek. "Navier-Stokes Predictions of Pitch Damping for Finned Projectiles Using Steady Coning Motion," AIAA Paper 90-3088, August 1990.

Weinacht, P., W. Sturek, and L. Schiff. "Navier-Stokes Predictions of Pitch Damping for Axisymmetric Shell Using Steady Coning Motion," AIAA Paper 91-2855, August 1991.

Weinacht, P., W.B. Sturek, and P.A. Wooden. "Computational Study of Inbore and Inflight Heating for the 105mm, M774 Projectile Modified Swept Fin," ARBRL-MR-03377, U.S. Army Ballistic Research Laboratory/AARDCOM, Aberdeen Proving Ground, Maryland, August 1984. (AD A146568)

Zucrow, M.J., and J.D. Hoffman. Gas Dynamics, Vol. 1, John Wiley & Sons, 1976.

INTENTIONALLY LEFT BLANK.

LIST OF SYMBOLS

a	speed of sound
d	reference diameter of projectile
e	total energy per unit volume of fluid
$\bar{e_n}$	unit vector perpendicular to body surface
$\hat{E}_s, \hat{F}, \hat{G}$	inviscid flux vectors of transformed gas dynamic equations
$\hat{H}_c$	inviscid source term for cylindrical coordinate formulation of transformed gas dynamic equations
h	surface heat transfer coefficient
k	coefficent of conductivity
l	reference length
M	Mach number
n	distance along $\bar{e_n}$
P_r	Prandtl number for laminar flow
$\bar{q}$	vector of heat transfer rate per unit area in $\bar{n}$ direction
q	heat transfer rate from fluid to body per unit area
$\bar{Q}$	vector of dependent variables of gas dynamic equations
$\hat{Re}$	free-stream sonic Reynolds number, $\rho_\infty a_\infty d/\mu_\infty$
Re_m	free-stream Reynolds number based on a length of 1 meter, $\rho_\infty V_\infty l/\mu_\infty$
r	recovery factor based on boundary-layer edge conditions
r_f	recovery factor based on free-stream conditions
s	distance from wall in $\bar{n}$ direction
$\hat{S}$	viscosity vector of transformed gas dynamic equations
$\hat{S}_c$	viscous source term for cylindrical coordinate formulation of transformed gas dynamic equations
T	temperature
T_f	temperature factor
u, v, w	velocity components in x, y, z directions
u_τ	shear velocity
V	total velocity
x, y, z	physical Cartesian coordinates
y^+	boundary layer coordinate in $\bar{n}$ direction

Greek Symbols

γ	ratio of specific heats
κ	coefficient of thermal conductivity
μ	coefficient of dynamic viscosity
ν	coefficient of kinematic viscosity
ξ, η, ζ	transformed coordinates
ρ	density
τ	shear stress

Subscripts

atm	sea-level atmospheric condition
aw	adiabatic wall condition
e	boundary layer edge condition
o	stagnation, or total, condition
w	wall condition
1	condition at first grid point away from wall
∞	free-stream condition
$\|_{wall}$	evaluated at the wall (body surface)

No. of Copies	Organization
2	Administrator Defense Technical Info Center ATTN: DTIC-DDA Cameron Station Alexandria, VA 22304-6145
1	Commander U.S. Army Materiel Command ATTN: AMCAM 5001 Eisenhower Ave. Alexandria, VA 22333-0001
1	Director U.S. Army Research Laboratory ATTN: AMSRL-OP-CI-AD, Tech Publishing 2800 Powder Mill Rd. Adelphi, MD 20783-1145
1	Director U.S. Army Research Laboratory ATTN: AMSRL-OP-CI-AD, Records Management 2800 Powder Mill Rd. Adelphi, MD 20783-1145
2	Commander U.S. Army Armament Research, Development, and Engineering Center ATTN: SMCAR-IMI-I Picatinny Arsenal, NJ 07806-5000
2	Commander U.S. Army Armament Research, Development, and Engineering Center ATTN: SMCAR-TDC Picatinny Arsenal, NJ 07806-5000
1	Director Benet Weapons Laboratory U.S. Army Armament Research, Development, and Engineering Center ATTN: SMCAR-CCB-TL Watervliet, NY 12189-4050
1	Director U.S. Army Advanced Systems Research and Analysis Office (ATCOM) ATTN: AMSAT-R-NR, M/S 219-1 Ames Research Center Moffett Field, CA 94035-1000

No. of Copies	Organization
1	Commander U.S. Army Missile Command ATTN: AMSMI-RD-CS-R (DOC) Redstone Arsenal, AL 35898-5010
1	Commander U.S. Army Tank-Automotive Command ATTN: AMSTA-JSK (Armor Eng. Br.) Warren, MI 48397-5000
1	Director U.S. Army TRADOC Analysis Command ATTN: ATRC-WSR White Sands Missile Range, NM 88002-5502
(Class. only) 1	Commandant U.S. Army Infantry School ATTN: ATSH-CD (Security Mgr.) Fort Benning, GA 31905-5660
(Unclass. only) 1	Commandant U.S. Army Infantry School ATTN: ATSH-WCB-O Fort Benning, GA 31905-5000
1	WL/MNOI Eglin AFB, FL 32542-5000
	Aberdeen Proving Ground
2	Dir, USAMSAA ATTN: AMXSY-D AMXSY-MP, H. Cohen
1	Cdr, USATECOM ATTN: AMSTE-TC
1	Dir, ERDEC ATTN: SCBRD-RT
1	Cdr, CBDA ATTN: AMSCB-CII
1	Dir, USARL ATTN: AMSRL-SL-I
10	Dir, USARL ATTN: AMSRL-OP-CI-B (Tech Lib)

DISTRIBUTION LIST

No. of Copies	Organization
12	Commander US Army Armament RD&E Center ATTN: SMCAR-AET-A, R. Kline S. Kahn C. Ng M. Amoruso H. Hudgins J. Grau E. Brown B. Wong W. Toledo S. Chung C. Livecchia G. Malejko Picatinny Arsenal, NJ 07806-5000
2	Commander US Army Armament RD&E Center ATTN: SMCAR-CCH-V, E. Fennell T. Louzeiro Picatinny Arsenal, NJ 07806-5000
2	Commander US Army Armament RD&E Center ATTN: SMCAR-FSE, D. Ladd E. Andricopoulos Picatinny Arsenal, NJ 07806-5000
1	Commander US Army Missile Command ATTN: AMSMI-RD-SS-AT, B. Walker Redstone Arsenal, AL 35898-5010
3	U.S. Army Research Office ATTN: G. Anderson K. Clark T. Doligowski P.O. Box 12211 Research Triangle Park, NC 27709-2211
2	Director US Army ERDEC ATTN: SCBRD-RTB, D. Weber F. Wrede Aberdeen Proving Ground, MD 21010-5423
2	Director US Army Research Laboratory ATTN: AMSRL-MA-CA, M.R. Fletcher M.E. O'Day 405 Arsenal St. Watertown, MA 02172-0001
1	United States Military Academy Department of Mechanics ATTN: A. Dull West Point, NY 10996
6	Director National Aeronautics and Space Administration *Ames Research Center* ATTN: MS-258-1, L. Schiff T. Holst D. Chaussee T. Edwards G. Molvik S. Lawrence Moffett Field, CA 94035
3	Director National Aeronautics and Space Administration Langley Research Center ATTN: Technical Library J. South M .Rai Langley Station Hampton, VA 23665
3	Air Force Armament Laboratory ATTN: AFATL/FXA, B. Simpson G. Abate R. Adelgren Eglin AFB, FL 32542-5434

DISTRIBUTION LIST

No. of Copies	Organization
2	Commander Naval Surface Warfare Center Applied Mathematics Branch ATTN: Code R44, A. Wardlaw Code R44, F. Priolo White Oak Laboratory Silver Spring, MD 20903-5000
1	Commander US Naval Surface Weapons Center ATTN: F. Moore Dahlgren, VA 22448
2	USAF Wright Aeronautical Laboratories ATTN: AFWAL/FIMG, J. Shang WPAFB, OH 45433-6553
1	Arnold Engineering & Development Center Calspan Field Service ATTN: MS 600, J. Benek AAFS, TN 37389
2	Director Sandia National Laboratories ATTN: W. Oberkampf W. Wolfe Division 1636 Albuquerque, NM 87185
1	Los Alamos National Laboratory ATTN: MS G770, W. Hogan Los Alamos, NM 87545
2	Institute for Advanced Technology University of Texas at Austin ATTN: W. Reinecke T. Kiehne 4030-2 W. Braker Lane Austin, TX 78759-5329
2	University of California, Davis Department of Mechanical Engineering ATTN: H. Dwyer B. Meakin Davis, CA 95616
1	University of Maryland Department of Aerospace Engr. ATTN: J. Anderson, Jr. College Park, MD 20742
1	University of Texas Department of Aerospace Engineering and Engineering Mechanics ATTN: D. Dolling Austin, Texas 78712-1055
1	University of Delaware Department of Mechanical Engineering ATTN: L. Schwartz Newark, DE 19716
1	University of Cincinnati Department of Aerospace Engineering ATTN: S. Rubin Mail Location 70 Cincinnati, OH 45221
1	University of Florida Department of Engineering Sciences College of Engineering ATTN: C. Hsu Gainesville, FL 32611
1	MDA Engineering, Inc. ATTN: J. Steinbrenner 500 E. Border St., Suite 401 Arlington, TX 76010
2	Alliant Techsystems, Inc. ATTN: M. Swenson R. Burretta Mail Station MN48-3700 7225 Northland Dr. Brooklyn Park, MN 55428
1	General Research Corp. ATTN: H.H. King P.O. Box 6770 Santa Barbara, CA 93160-6770

INTENTIONALLY LEFT BLANK.

USER EVALUATION SHEET/CHANGE OF ADDRESS

This Laboratory undertakes a continuing effort to improve the quality of the reports it publishes. Your comments/answers to the items/questions below will aid us in our efforts.

1. ARL Report Number ARL-TR-191 Date of Report August 1993

2. Date Report Received _____

3. Does this report satisfy a need? (Comment on purpose, related project, or other area of interest for which the report will be used.) _____

4. Specifically, how is the report being used? (Information source, design data, procedure, source of ideas, etc.) _____

5. Has the information in this report led to any quantitative savings as far as man-hours or dollars saved, operating costs avoided, or efficiencies achieved, etc? If so, please elaborate. _____

6. General Comments. What do you think should be changed to improve future reports? (Indicate changes to organization, technical content, format, etc.) _____

CURRENT ADDRESS

_____
Organization

_____
Name

_____
Street or P.O. Box No.

_____
City, State, Zip Code

7. If indicating a Change of Address or Address Correction, please provide the Current or Correct address above and the Old or Incorrect address below.

OLD ADDRESS

_____
Organization

_____
Name

_____
Street or P.O. Box No.

_____
City, State, Zip Code

(Remove this sheet, fold as indicated, tape closed, and mail.)
(DO NOT STAPLE)

DEPARTMENT OF THE ARMY

OFFICIAL BUSINESS

BUSINESS REPLY MAIL
FIRST CLASS PERMIT No 0001, APG, MD

Postage will be paid by addressee.

Director
U.S. Army Research Laboratory
ATTN: AMSRL-OP-CI-B (Tech Lib)
Aberdeen Proving Ground, MD 21005-5066

NO POSTAGE
NECESSARY
IF MAILED
IN THE
UNITED STATES